Status of the Tibetan Plateau observatory (Tibet-Obs) and a 10-year (2009-2019) surface soil moisture dataset

Pei Zhang[1,2], Donghai Zheng[2], Rogier van der Velde[1], Jun Wen[3], Yijian Zeng[1], Xin Wang[4], Zuoliang Wang[4], Jiali Chen[2,5], Zhongbo Su[1]

[1]Faculty of Geo-Information Science and Earth Observation (ITC), University of Twente, Enschede, 7514AE, the Netherlands
[2]National Tibetan Plateau Data Center, Key Laboratory of Tibetan Environmental Changes and Land Surface Processes, Institute of Tibetan Plateau Research, Chinese Academy of Sciences, Beijing, 100101, China
[3]College of Atmospheric Sciences, Chengdu University of Information Technology, Chengdu, 610225, China
[4]Northwest Institute of Eco-Environment and Resources, Chinese Academy of Sciences, Lanzhou, 730000, China
[5]College of Earth and Environmental Sciences, Lanzhou University, Lanzhou, 730000, China

Correspondence to: Donghai Zheng (zhengd@itpcas.ac.cn),Z. (Bob) Su (z.su@utwente.nl)

Abstract. The Tibetan Plateau observatory of plateau scale soil moisture and soil temperature (Tibet-Obs) was established ten years ago, which has been widely used to calibrate/validate satellite- and model-based soil moisture (SM) products for their applications to the Tibetan Plateau (TP). This paper reports on the status of the Tibet-Obs and presents a 10-year (2009-2019) surface SM dataset produced based on *in situ* measurements taken at a depth of 5 cm collected from the Tibet-Obs that consists of three regional-scale SM monitoring networks, i.e. the Maqu, Naqu, and Ngari (including Ali and Shiquanhe) networks. This surface SM dataset includes the original 15-min *in situ* measurements collected by multiple SM monitoring sites of the three networks, and the spatially upscaled SM records produced for the Maqu and Shiquanhe networks. Comparisons between four spatial upscaling methods, i.e. arithmetic averaging, Voronoi diagram, time stability, and apparent thermal inertia, show that the arithmetic average of the monitoring sites with long-term (i.e. ≥ six years) continuous measurements are found to be most suitable to produce the upscaled SM records. Trend analysis of the 10-year upscaled SM records indicates that the Shiquanhe network area in the western part of the TP is getting wet while there is not significant trend found for the Maqu network area in the east. To further demonstrate the uniqueness of the upscaled SM records in validating existing SM products for long term period (~10 years), comparisons are conducted to evaluate the reliability of three reanalysis datasets for the Maqu and Shiquanhe network areas. It is found that current model-based SM products still show deficiencies in representing the trend and variation of measured SM dynamics in the Tibetan grassland (i.e. Maqu) and desert ecosystems (i.e. Shiquanhe) that dominate the landscape of the TP. The dataset would be also valuable for calibrating/validating long-term satellite-based SM products, evaluation of SM upscaling methods, development of data fusion methods, and quantifying the coupling strength between precipitation and SM at 10-year scale. The dataset is available in the 4TU.ResearchData repository at https://doi.org/10.4121/uuid:21220b23-ff36-4ca9-a08f-ccd53782e834 (Zhang et al., 2020).

1 Introduction

The Tibetan Plateau observatory (Tibet-Obs) of plateau scale soil moisture and soil temperature (SMST) was setup in 2006 and became fully operational in 2010 to calibrate/validate satellite- and model-based soil moisture (SM) products at regional scale (Su et al., 2011). The Tibet-Obs mainly consists of three regional-scale SMST monitoring networks, i.e. Maqu, Naqu, and Ngari, which cover different climate and land surface conditions across the Tibetan Plateau (TP) and include multiple *in situ* SMST monitoring sites in each network. The SM data collected from the Tibet-Obs have been widely used in past decade to calibrate/validate satellite- and model-based SM products (e.g. Su et al., 2013; Zheng et al., 2015a; Colliander et al., 2017), and to evaluate and develop SM upscaling methods (e.g. Qin et al., 2013; 2015), SM retrieval algorithms for microwave remote sensing (e.g. van der Velde et al., 2012; 2014a; Zheng et al., 2018a; 2018b; 2019), and fusion methods to merge *in situ* SM and satellite- or model-based products (e.g. Yang et al., 2020; Zeng et al., 2016).

Key information and outcomes of the main scientific applications using the Tibet-Obs SM data are summarized in Table 1. As shown in Table 1, the state-of-the-art satellite- and model-based products are useful but still show deficiencies of different degrees in different hydrometeorological conditions on the TP, and further evaluation and improvement of the latest versions of these products remain imperative. In general, previous studies mainly focused on the evaluation of SM products using the Tibet-Obs data for short term period (i.e. less than five years), while up to now the Tibet-Obs have collected *in situ* measurements more than 10 years. Development of an approximate 10-year *in situ* SM dataset collected from the Tibet-Obs would further enhance the calibration/validation of long-term satellite- and model-based products, and should be valuable for better understanding the hydrometeorological response to climate changes. However, the SM is highly variable in both space and time, and data gaps in the availability of measurements taken from individual monitoring site hinder scientific studies of longer periods, e.g. more than five years. Therefore, it is still challenging to obtain accurate long-term regional-scale SM due to the sparse nature of monitoring networks and highly variable soil conditions.

Spatial upscaling is usually necessary to obtain the regional-scale SM of an *in situ* network from multiple monitoring sites to match the footprint-scale of satellite- or model-based products. A frequently used approach for upscaling point-scale SM measurements to a spatial domain is the arithmetic average, mostly because of its simplicity (Su et al. 2011; 2013). Many other studies also adopted the weighted averaging methods, whereby the weights are assigned to account for spatial heterogeneity within the network areas covered by *in situ* monitoring sites. For instance, Colliander et al. (2017) employed Voronoi diagrams for the worldwide validation of the Soil Moisture Active/Passive (SMAP) SM products to determine the weights of individual monitoring sites within core regional-scale networks based on the geographic location; Dente et al. (2012a) determined the weights based on the topography and soil texture for the Maqu SM monitoring network of the Tibet-Obs; Qin et al. (2013, 2015) derived the weights by minimizing a cost function between *in situ* SM of individual monitoring site and a representative SM of the network that is estimated using the apparent-thermal-inertia-based (ATI) method (Gao et al., 2017). Alternative methods, such as time stability

and ridge regression, have been adopted in other investigations (i.e. Zhao et al., 2013, Kang et al., 2017). While a large number of studies have assessed the performance of different upscaling methods in other areas such as the Tonzi Ranch network in California and the Heihe watershed (Moghaddam et al., 2014, Wang et al., 2014), only few investigations have been done for the TP (Gao et al., 2017, Qin et al., 2015). Since the number of monitoring sites changes over time due to damage of SM sensors in the Tibet-Obs, it is essential to evaluate and select an appropriate upscaling method for a limited number of monitoring sites.

This paper reports on the status of the Tibet-Obs and presents a long-term *in situ* SM and spatially upscaled SM dataset for the period between 2009 and 2019. The 10-year SM dataset includes the original 15-min *in situ* measurements taken at a depth of 5 cm collected from the three regional-scale networks (i.e. Maqu, Naqu, and Ngari as shown in Fig. 1) of the Tibet-Obs, and the consistent regional-scale SM produced by an appropriately selected spatial upscaling method. To achieve this aim, four methods are used in this study including the arithmetic averaging (AA), Voronoi diagram (VD), time stability (TS), and apparent thermal inertia (ATI) methods. Moreover, the variation and trend of the regional-scale SM time series are analyzed, and this 10-year SM dataset is used to validate the performance of three model-based SM products, e.g. ERA5-land (Muñoz-Sabater et al., 2018), MERRA2 (Modern-Era Retrospective Analysis for Research and Applications, version 2) (GMAO, 2015), and GLDAS Noah (Global Land Data Assimilation System with Noah Land Surface Model) (Rodell et al., 2004), to demonstrate the uniqueness of this dataset for validating existing reanalysis datasets for a long term period (~10 years).

This paper is organized as follows. Section 2 describes the status of the Tibet-Obs and *in situ* SM measurements, as well as the precipitation data and the three model-based SM products. Section 3 introduces the four SM spatial upscaling methods, Mann Kendall trend test and Sen's slope estimate, and statistical metrics. Section 4 presents the inter-comparison of the four SM spatial upscaling methods, the production and analysis of regional-scale SM dataset for a 10-year period, and its application to validate the three model-based SM products. Section 5 provides the discussion and suggestion on maintaining the Tibet-Obs. Section 6 documents the information of data availability. Finally, conclusions are drawn in Section 7.

2 Data

2.1 Status of the Tibet-Obs

The Tibet-Obs consists of the Maqu, Naqu, and Ngari (including Shiquanhe and Ali) regional-scale SMST monitoring networks (Fig. 1) that cover the cold humid climate, cold semiarid climate, and cold arid climate, respectively. Each network includes different number of monitoring sites that measure the SMST at different soil depths. Brief descriptions of each network and corresponding surface SM measurements taken at a depth of 5 cm are given in following subsections. The readers are referred to existing literatures (Su et al., 2011; Dente et al. 2012a; Zhao et al., 2018) for additional information of networks.

2.1.1 Maqu network

The Maqu network is located in the north-eastern edge of the TP (33°30'-34°15'N, 101°38'-102°45'E) at the first major bend of the Yellow River. The landscape is dominated by the short grass at elevations varying from 3400 to 3800 m. The climate type is characterized as cold-humid with cold dry winters and rainy summers. The mean annual air temperature is about 1.2 ℃, with -10 ℃ for the coldest month (January) and 11.7 ℃ for the warmest month (July) (Zheng et al., 2015a).

The Maqu network covers an area of approximately 40 by 80 km^2 and consists originally of 20 SMST monitoring sites installed in 2008 (Dente et al. 2012a). During the period between 2014 and 2016, eight new sites were installed due to the damage of several old monitoring sites by local people or animals. The basic information of each monitoring site is summarized in Table A1 (Su et al., 2011), and the typical characteristics of topography and land cover within the network are shown in Fig. 2 as well. The Decagon 5TM ECH$_2$O probes were used to measure the SMST at depths of 5, 10, 20, 40, and 80 cm (Fig. 3). The 5TM probe is a capacitance sensor measuring the dielectric permittivity of soil, and the Topp equation (Topp et al., 1980) is used to convert the dielectric permittivity to the volumetric SM. The accuracy of the 5TM output was further improved via a soil-specific calibration performed for each soil type found in the Maqu network area (Dente et al. 2012a), leading to a decrease in the root mean square error (RMSE) from 0.06 to 0.02 m^3 m^{-3} (Dente et al. 2012a). Table 2 provides the specific periods of data missing during each year and the total data lengths of surface SM for each monitoring site. Among these sites, the CST05, NST01, and NST03 have collected more than nine years of SM measurements, while the data records for the NST21, NST22, and NST31 are less than one year. In May 2019, there are still 12 monitoring sites that provided SM data.

2.1.2 Ngari network

The Ngari network is located in the western part of the TP at the headwater of the Indus River. It consists of two SMST networks established around the cities of Ali and Shiquanhe, respectively. The landscape is dominated by a desert ecosystem at elevations varying from 4200 to 4700 m. The climate type is characterized as cold-arid with a mean annual air temperature of 7.0 ℃. The annual precipitation is less than 100 mm that falls mainly in the monsoon season (July-August) (van der Velde et al., 2014).

The Shiquanhe network consists originally of 16 SMST monitoring sites installed in 2010 (Su et al. 2011), and five new sites were installed in 2016. The basic information of each monitoring site is summarized in Table A3 (Su et al., 2011), and the typical characteristics of topography and land cover within the network are also shown in Fig. 4. The Decagon 5TM ECH$_2$O probes were installed at depths of 5, 10, 20, 40, and 60/80 cm to measure the SMST (Fig. 3). Table 3 provides the specific periods of data missing during each year and the total data lengths of surface SM for each site. Among these sites, the SQ02, SQ03, SQ06, and SQ14 have collected more than eight years of SM measurements, while the data records for the SQ13, SQ15, and SQ18 are less than two years. In August 2019, there are still 12 sites that provided SM data. The Ali network comprise four SM monitoring sites (Table A3), which will thus not be used for the further analysis in this study due to limited number of monitoring sites and data records (Table 3).

144 **2.1.3 Naqu network**

145 The Naqu network is located in the Naqu river basin with an average elevation of 4500 m. The climate type

146 is characterized as cold-semiarid with cold dry winters and rainy summers. Over three-quarters of total annual

147 precipitation (400 mm) falls between June and August (Su et al., 2011). The landscape is dominated by the

148 short grass.

149 The network consists originally of five SMST monitoring sites installed in 2006 (Su et al. 2011), and six new

150 sites were installed between 2010 and 2016. The basic information of each monitoring site is summarized in

151 Table A5, and the typical characteristics of topography and land cover within the network are shown in Fig.

152 5 as well. The Decagon 5TM ECH$_2$O probes were installed at depths of 5/2.5, 10/7.5, 15, 30, and 60 cm to

153 measure the SMST, and the soil-specific calibration was also performed by van der Velde (2010) that yields

154 a RMSE of about 0.029 m^3 m^{-3}. Table 4 provides the specific periods of data missing during each year and

155 the total data lengths of surface SM for each site. Among these sites, only two sites (Naqu and MS sites in

156 Table A5) have collected more than six years of SM measurements, while the data records for the others are

157 less than four years. Similar to the Ali network, the Naqu network will also not be used for the further analysis

158 in this study due to limited number of monitoring sites and data records.

159 **2.2 Precipitation data**

160 The precipitation data is from two weather stations, i.e. Maqu (34°00'N, 102°05'E) and Shiquanhe (32°30'N,

161 80°05'E), operated by the China Meteorological Administration (CMA) which provides the near-surface

162 meteorological data of about 700 weather stations in China. The daily precipitation data can be downloaded

163 from https://data.cma.cn/dataService/cdcindex/datacode/SURF_CLI_CHN_MUL_DAY.html that is in

164 Chinese. The data is only available to agreement users, which is not allowed to be shared without permission

165 from the CMA.

166 **2.3 Model-based soil moisture products**

167 **2.3.1 ERA5-land soil moisture product**

168 ERA5-land is a reanalysis dataset produced by running land component of the ECMWF (European Centre

169 for Medium-Range Weather Forecasts) ERA5 climate reanalysis (Albergel et al., 2018). ERA5-land provides

170 SM data currently available from 1981 to present at hourly time interval with a spatial resolution of 0.1°, and

171 the data is available from https://cds.climate.copernicus.eu/cdsapp#!/dataset/reanalysis-era5-land?tab (last

172 verified on 11 March 2021). More information about the ERA5-land product can be referred to Muñoz-

173 Sabater et al., (2018). In this study, the data of volumetric total soil water content for the top soil layer (0-7

174 cm) is used for the analysis.

175 **2.3.2 MERRA2 soil moisture product**

176 MERRA2 is an atmospheric reanalysis dataset produced by NASA using the Goddard Earth Observing

177 System Model version 5 (GEOS-5) and atmospheric data assimilation system (ADAS), version 5.12.4.

178   MERRA2 provides SM data currently available from 1980 to present at hourly time interval with a spatial

179   resolution of 0.5° (latitude) by 0.625° (longitude), and the data is available from

180   https://disc.gsfc.nasa.gov/datasets/M2T1NXLND_5.12.4/summary (last verified on 11 March 2021). More

181   information about the MERRA2 product can be referred to GMAO (2015). In this study, the data of

182   volumetric liquid soil water content for the surface layer (0-5 cm) is used for the analysis.

183 2.3.3 GLDAS Noah soil moisture product

184   GLDAS-2.1 Noah is forced by a combination of model-based and observation data including Global

185   Precipitation Climatology Project (GPCP) version 1.3, and simulated with the Noah Model 3.6 in Land

186   Information System (LIS) version 7. GLDAS-2.1 Noah provides SM data currently available from 2000 to

187   present at 3-hourly time interval with a spatial resolution of 0.25°, and the data is available from

188   https://disc.gsfc.nasa.gov/datasets/GLDAS_NOAH025_3H_2.1/summary (last verified on 11 March 2021).

189   More information about the GLDAS Noah product can be referred to Rodell et al. (2004). In this study, the

190   data of soil water content for the top soil layer (0-10 cm) is used for the analysis.

191 3 Methods

192 3.1 Spatial upscaling of soil moisture measurements

193   The principle of spatial upscaling method is to determine the weight for each SM monitoring site with the

194   aid of extra information. The method generally follows the linear functional form, which can be

195   mathematically defined as:

196    $\overline{\theta}_t^{ups} = \theta_t^{obs}\beta$ (1a)

197    $\theta_t^{obs} = [\theta_{t,1}^{obs}, \theta_{t,2}^{obs}, \dots, \theta_{t,N}^{obs}]^T$ (1b)

198   where $\overline{\theta}_t^{ups}$[m^3 m^{-3}] represents the upscaled SM, θ_t^{obs}[m^3 m^{-3}] represents the vector of SM measurements, N

199   represents the total number of SM monitoring sites, t represents the time (e.g. the tth day), and β [-] represents

200   the weight vector.

201   In this study, only the surface SM measurements taken from the Maqu and Shiquanhe networks are upscaled

202   to obtain the regional-scale SM for a long-term period due to the availability of much longer data records in

203   comparison to the Naqu and Ali networks (see Section 2.1). Four upscaling methods are investigated and

204   inter-compared with each other to find the most suitable method for the application to the Tibet-Obs. Brief

205   descriptions of the selected upscaling methods are given in Appendix B. The arithmetic averaging method

206   (hereafter "AA") assigns an equal weight coefficient to each SM monitoring site (see Appendix B.1), while

207   the Voronoi diagram method (hereafter "VD") determines the weight based on the geographic distribution

208   of all the SM monitoring sites (see Appendix B.2). On the other hand, the time stability method (hereafter

209   "TS") regards the most stable site as the representative site of the SM monitoring network (see Appendix

210   B.3), while the apparent thermal inertia (ATI) method is based on the close relationship between apparent

211   thermal inertia (τ) and SM (see Appendix B.4).

3.2 Trend analysis

The Mann-Kendall test and Sen's slope estimate (Gilbert, 1987; Mann, 1945; Smith et al., 2012) are adopted in this study to analyze the trend of 10-year upscaled SM time series and model-based products (i.e. ERA5-land, GLDAS Noah, and MERRA2). Specifically, the trend analysis is based on the monthly average SM, and all the missing data is regarded as an equal value smaller than other valid data. The test consists of calculating the seasonal statistics S and its variance VAR(S) separately for each month during the 10-year period, and the seasonal statistics are then summed to obtain the Z statistics.

For the month i (e.g. January), the statistics S_i can be computed as:

$$S_i = \sum_{k=1}^{9} \sum_{l=k+1}^{10} sgn(SM_{i,l} - SM_{i,k}) \tag{2a}$$

$$sgn(SM_{i,l} - SM_{i,k}) = \begin{cases} 1 & SM_{i,l} > SM_{i,k} \\ 0 & SM_{i,l} = SM_{i,k} \\ -1 & SM_{i,l} < SM_{i,k} \end{cases} \tag{}$$

where k and l represent the different year and $l > k$, $SM_{i,l}$ and $SM_{i,k}$ represent the monthly average SM for the month i of the year k and l, respectively.

The $VAR(S_i)$ is computed as:

$$VAR(S_i) = \frac{1}{18} [N_i(N_i - 1)(2N_i + 5) - \sum_{p=1}^{g_i} t_{i,p}(t_{i,p} - 1)(2t_{i,p} + 5)] \tag{2b}$$

where N_i is the length of the record for the month i (e.g. the 10 year data record in this study with $N_i=10$), g_i is the number of equal-value data in month i, $t_{i,p}$ is the number of equal-value data in the pth group for month i.

After obtaining the S_i and $VAR(S_i)$, the statistic S' and $VAR(S')$ for the selected season (e.g. warm season between May and October and cold season between November and April in this study) can be summed as:

$$S' = \sum_{i=1}^{M} S_i \tag{2c}$$

$$VAR(S') = \sum_{i=1}^{M} VAR(S_i) \tag{2d}$$

where M represents the number of months in the selected season, e.g. M = 12 for the full year, while M = 6 for the warm and cold season, respectively.

Then the statistics Z can be computed as:

$$Z = \begin{cases} \frac{S'-1}{\sqrt{Var(S')}} & if\ S' > 0 \\ 0 & if\ S' = 0 \\ \frac{S'+1}{\sqrt{Var(S')}} & if\ S' < 0 \end{cases} \tag{2e}$$

If the statistics Z is positive (negative) and its absolute value is greater than $Z_{1-\alpha/2}$ (here $\alpha = 0.05$, $Z_{1-\alpha/2} = 1.96$), the trend of the SM time series is regarded as upward (downward) at the significance level of α. Otherwise, we accept the hypothesis that there is not significant trend found for the SM time series.

If the trend is monotonous, we will further estimate the slope (change per unit time) with Sen's method (Sen, 1968). The slopes of each month can be calculated as:

$$Q_i = \frac{SM_{i,l} - SM_{i,k}}{l-k} \tag{2f}$$

243   Then rank all the individual slopes (Q_i) for all months and find the median which is considered as the

244   seasonal Kendall slope estimate.

245   **3.3 Metrics used for statistical comparison**

246   The metrics used to evaluate the accuracy of the upscaled SM are the bias [m^3 m^{-3}], RMSE [m^3 m^{-3}], and

247   unbiased RMSE (ubRMSE [m^3 m^{-3}]) as:

248    $\text{Bias} = \frac{\sum_{t=1}^{M}(\theta_t^{tru} - \overline{\theta}_t^{ups})}{M}$ (3a)

249    $\text{RMSE} = \sqrt{\frac{\sum_{t=1}^{M}(\theta_t^{tru} - \overline{\theta}_t^{ups})^2}{M}}$ (3b)

250    $\text{ubRMSE} = \sqrt{RMSE^2 - BIAS^2}$ (3c)

251   where θ_t^{tru} represents the SM that is considered as the ground truth, and $\overline{\theta}_t^{ups}$ represents the upscaled SM.

252   The closer the metric is to zero, the more accurate the estimation is.

253   The metrics used for the correlation analysis are the Nash-Sutcliffe efficiency coefficient (NSE [-]) as:

254    $\text{NSE} = 1 - \frac{\sum_{t=1}^{n}(\theta_t^{tru} - \overline{\theta}_t^{ups})^2}{\sum_{t=1}^{n}(\theta_t^{tru} - \overline{\theta_t^{tru}})^2}$ (4)

255   The value of the NSE ranges from -∞ to 1, and the closer the metric is to 1, the better the match of the

256   estimated SM with the reference (θ_t^{tru}).

257   The metrics used to define the most representative SM time series (i.e. the best upsclaed SM) is the

258   comprehensive evaluation criterion (*CEC* [-]) combined by two statistical metrics including relative

259   difference (*MRD* [-]) and standard deviation of the relative difference ($\sigma(RD)$ [-]) (Jacobs et al., 2004).

260   Detailed description of above mentioned three metrics are given in Appendix B.3. It should be noted that the

261    $\theta_{t,i}^{obs}$ and $\overline{\theta_t^{obs}}$ in Eqs. (B4) and (B5) represent the upscaled SM using four different methods and their average

262   here when using the *CEC* to determine the best upscaled SM. The most representative time series is identified

263   by the lowest *CEC* value.

264   **3.4 Preprocessing of model-based soil moisture products**

265   The performance of the ERA5-land, MERRA2, and GLDAS Noah SM products are assessed using the

266   upscaled SM data of the Maqu and Shiquanhe networks for a 10-year period. The corresponding regional-

267   scale SM for each product can be obtained by averaging the grid data falling in the network areas. The

268   numbers of grids covering the Maqu and Shiquanhe networks are 77 and 20 for the ERA5-land product, 12

269   and 4 for the GLDAS Noah product, and only one for the MERRA2 product. Moreover, the ERA5-land and

270   MERRA2 products with the temporal resolution of hourly and 3-hourly are averaged to daily-scale, and the

271   unit of GLDAS Noah SM is converted from kg m^{-2} to m^3 m^{-3}. The uppermost layer of the ERA5-land (0-7

272   cm), MERRA2 (0-5 cm), and GLDAS Noah (0–10 cm) SM products are considered to match the *in situ*

273   observations at depth of 5 cm.

274   **4 Results**

275   **4.1 Inter-comparison of soil moisture upscaling methods**

276   In this section, four upscaling methods (see Section 3.1) are inter-compared first with the input of the

277   maximum number of available SM monitoring sites for a single year in the Maqu and Shiquanhe networks

278   to find the most suitable upscaled SM that can best represent the areal conditions (i.e. ground truth, SM_{truth}).

279   Later on, the performance of the four upscaling methods is further investigated with the input of reducing

280   number of SM monitoring sites to find the most suitable method for producing long-term (~10 year) upscaled

281   SM for the Maqu and Shiquanhe networks.

282   Fig. 6 shows the time series of daily average SM for the Maqu and Shiquanhe networks produced by the four

283   upscaling methods based on the maximum number of available SM monitoring sites (hereafter "$SM_{AA\text{-}max}$",

284   "$SM_{VD\text{-}max}$", "$SM_{TS\text{-}max}$", and "$SM_{ATI\text{-}max}$"). Two different periods are selected for the two networks due to the

285   fact that the number of available monitoring sites reaches the maximum in different periods for the two

286   networks, e.g. 17 sites for Maqu between November 2009 and October 2010 and 12 sites for Shiquanhe

287   between August 2018 and July 2019, respectively (see Tables A2 and A4 in the Appendix A). For the Maqu

288   network, the $SM_{AA\text{-}max}$, $SM_{VD\text{-}max}$, and $SM_{TS\text{-}max}$ are comparable to each other, while the $SM_{ATI\text{-}max}$ shows

289   distinct deviations during the winter (between December and February) and summer periods (between June

290   and August). On the other hand, the $SM_{ATI\text{-}max}$ for the Shiquanhe network is comparable to $SM_{AA\text{-}max}$ and

291     $SM_{VD\text{-}max}$, while deviation is observed for the $SM_{TS\text{-}max}$. It seems that the ATI method performs better in the

292   Shiquanhe network due to the existence of a stronger relationship between τ and θ in the desert ecosystem.

293   Table B1 lists the values of *MRD* (see Eq. (B4) in Appendix B), $\sigma(RD)$ (Eq. (B3)), and *CEC* (Eq. (B6))

294   calculated for the upscaled SM produced by the four upscaling methods. The *CEC* is used here to determine

295   the most suitable upscaled SM that can best represent the areal conditions for the two networks. It can be

296   found that the $SM_{AA\text{-}max}$ yields the lowest *CEC* values for both networks, indicating that the $SM_{AA\text{-}max}$ can be

297   used to represent actual areal conditions, which will thus be regarded as the ground truth for following

298   analysis (i.e. SM_{truth}). The arithmetic average of the dense *in situ* measurements was also used as the ground

299   truth in other studies (Qin et al., 2013; Su et al., 2013).

300   As shown in Tables A2 and A4 (see Appendix A), the number of available SM monitoring sites decreases

301   with increasing time span of *in situ* measurements. There are only three (i.e. CST05, NST01, and NST03)

302   and four (i.e. SQ02, SQ03, SQ06, and SQ14) monitoring sites that provided more than nine years of *in situ*

303   SM measurement data for the Maqu and Shiquanhe networks, respectively (see Tables 2 and 3). This

304   indicates that the minimum number of available monitoring sites can be used to produce the long-term (~10

305   year) consistent upscaled SM are three and four for the Maqu and Shiquanhe networks, respectively. Fig. 7

306   shows the daily average SM time series produced by the four upscaling methods based on the minimum

307   available monitoring sites (hereafter "AA-min", "TS-min", "VD-min", and "ATI-min"). The SM_{truth} obtained

308   by the AA-max is also shown for comparison purpose. For the Maqu network, the upscaled SM produced by

309   the AA-min, VD-min, and TS-min generally capture well the SM_{truth} variations, while the upscaled SM of

310   the ATI-min shows dramatic deviations. Similarly, the upscaled SM produced by the AA-min and VD-min

311   are consistent with the SM_{truth} for the Shiquanhe network with slight overestimations, while significant

312   deviations are noted for the upscaled SM of the TS-min and ATI-min. Table B2 lists the error statistics (e.g.

313   Bias, RMSE, ubRMSE, and NSE) computed between the upscaled SM produced by these four upscaling

314   methods with the input of the minimum available sites and the SM_{truth}. The upscaled SM produced by the

315   AA-min shows better performance for both networks as indicated by the lower RMSE and higher NSE values

316   in comparison to the other three upscaling methods.

317   Apart from the maximum and minimum numbers of available SM monitoring sites mentioned above, there

318   are about 14, 10, 8, and 6 available monitoring sites during different time spans for the Maqu network, and

319   for the Shiquanhe network are about 11, 10, 6, and 5 available monitoring sites (see Tables A2 and A4 in the

320   Appendix A). Fig. B2 shows the radar graph of error statistics (i.e. RMSE and NSE) computed between the

321   SM_{truth} and the upscaled SM produced by the four upscaling methods based on the input of different numbers

322   of available monitoring sites. For the Maqu network, the performances of the AA and VD methods are better

323   than the TS and ATI methods as indicated by smaller RMSEs and higher NSEs for all the estimations. A

324   similar conclusion can be obtained for the Shiquanhe network, while the performance of the ATI method is

325   largely improved when the number of available monitoring sites is not less than 10. It is interesting to note

326   that the upscaled SM produced by the AA-min are comparable to those produced with more available sites

327   (e.g. 10 sites) as indicated by comparable RMSE and NSE values for both networks. It indicates that the AA-

328   min is suitable to produce long-term (~10 years) upscaled SM for both networks, which yield RMSEs of

329   0.022 and 0.011 m^3 m^{-3} for the Maqu and Shiquanhe networks in comparison to the SM_{truth} produced by the

330   AA-max based on the maximum available monitoring sites.

331   **4.2 Long-term analysis of upscaled soil moisture measurements**

332   In this section, the AA-min is first adopted to produce the consecutive upscaled SM time series (hereafter

333   "SM_{AA-min}") for an approximately 10-year period for the Maqu and Shiquanhe networks, respectively. In

334   addition, the other time series of upscaled SM are produced by the AA method with input of all available SM

335   monitoring sites regardless of the continuity (hereafter "$SM_{AA-valid}$"), which is widely used to validate the

336   various SM products (Dente et al. 2012a; Chen et al. 2013; Zheng et al. 2018b) for a short term period (e.g.

337   ≤ 2 years). This method may, however, leads to inconsistent SM time series for a long-term period due to the

338   fact that the number of available sites is different in distinct periods (see Tables A2 and A4 in the Appendix

339   A). Trend analysis (see Section 3.2) are applied to both SM_{AA-min} and $SM_{AA-valid}$ to investigate the impact of

340   change of available SM monitoring sites over time on the long-term (i.e. 10-year) trend.

341   Fig. 8a shows the time series of SM_{AA-min} and $SM_{AA-valid}$ along with the daily precipitation data for the Maqu

342   network during the period between May 2009 and May 2019. Both two time series of the SM show similar

343   seasonality with low values in winter due to frozen of soil and high values in summer due to rainfall (see

344   subplot of Fig. 8a). Deviations can be found between the SM_{AA-min} and $SM_{AA-valid}$ especially for the period

345   between 2014 and 2019, whereby the $SM_{AA-valid}$ tends to produce smaller SM values in the warm season. Fig.

346   9a shows further the Mann Kendall trend test and Sen's slope estimate for the SM_{AA-min}, $SM_{AA-valid}$, and

347   precipitation of the Maqu network area for the full year, warm seasons, and cold seasons in a 10-year period.

348   As described in Section 3.2, the time series would present a monotonous trend if the absolute value of

349   statistics Z is greater than a critical value, i.e. $Z_{0.05} = 1.96$ in this study. The results show that there is not

350   significant trend found for both precipitation and SM_{AA-min} time series, while the $SM_{AA-valid}$ shows a drying

351   trend with a Sen's slope of -0.008 for warm seasons. The drying trend of the $SM_{AA-valid}$ is caused by the

352   change of available SM monitoring sites (see Table A2). Specifically, several monitoring sites (e.g. NST11-

353   NST15) located in the wetter area were damaged since 2013, and four new monitoring sites (i.e. NST21-

354   NST25) were installed in the drier area in 2015 (see Table 2) that affect the trend of the $SM_{AA-valid}$.

355   Fig. 8b shows the time series of the SM_{AA-min} and $SM_{AA-valid}$ along with the daily precipitation data for the

356   Shiquanhe network during the period between August 2010 and August 2019. Both time series of the SM

357   show similar seasonal variations as the Maqu network (see subplot of Fig. 8b). However, obvious deviation

358   can be noted for the inter-annual variations, and the $SM_{AA-valid}$ tends to produce lager values before 2014 but

359   smaller values since then. The Mann Kendall trend test and Sen's slope estimate for the SM_{AA-min}, $SM_{AA-valid}$,

360   and precipitation time series of the Shiquanhe network area are shown in Fig. 9b. The SM_{AA-min} demonstrates

361   a wetting trend with a Sen's slope of 0.003, while an opposite drying tendency is found for the $SM_{AA-valid}$ due

362   to the change of available SM monitoring sites (see Table A4) as the Maqu network. Specifically, several

363   monitoring sites (e.g. SQ11 and SQ12) located in the wetter area were damaged around 2014, and five new

364   monitoring sites (i.e. SQ17-21) were installed in the drier area in 2016 (see Table 3).

365   In summary, the $SM_{AA-valid}$ are likely affected by the change of available SM monitoring sites over time that

366   leads to inconsistent trend with the SM_{AA-min}. This indicates that the SM_{AA-min} is superior to the $SM_{AA-valid}$ for

367   the production of the long-term consistent upscaled SM time series.

4.3 Application of the long-term upscaled soil moisture to validate the model-based products

369   In this section, the long-term upscaled SM time series (i.e. SM_{AA-min}) produced for the two networks are

370   applied to validate the reliability of three model-based SM products, i.e. ERA5-land, MERRA2, and GLDAS

371   Noah, to demonstrate the uniqueness of this dataset for validating existing reanalysis datasets for a long term

372   period (~10 years). Since the ERA5-land product only provides the data of volumetric total soil water content,

373   the period when the soil is subject to freezing and thawing transition (i.e. November-April) is excluded for

374   this evaluation.

375   Fig. 10a shows the time series of SM_{AA-min} and daily average SM data derived from the three products for the

376   Maqu network area during the period between May 2009 and May 2019. The error statistics, i.e. bias and

377   RMSE, computed between the three products and the SM_{AA-min} for both warm (May-October) and cold

378   seasons (November-April) are given in Table 5. Although the three products generally capture the seasonal

379   variations of the SM_{AA-min}, the magnitude of the temporal SM variability is underestimated. Both GLDAS

380   Noah and MERRA2 products underestimate the SM measurements during the warm season leading to bias

381   of about -0.112 and -0.113 m^3 m^{-3}, respectively. This may be due to the fact that the LSMs adopted for

382   producing these products do not consider the impact of vertical soil heterogeneity caused by organic matter

383 contents widely existed in the surface layer of the Tibetan soil (Chen et al., 2013; Zheng et al., 2015a). In

384 addition, the MERRA2 product overestimates the SM measurements during the cold season with bias of

385 about 0.006 m^3 m^{-3}. The ERA5-land product is able to capture the magnitude of SM_{AA-min} dynamics in the

386 warm season but with more fluctuation that yields a RMSE of about 0.067 m^3 m^{-3}. The trend analysis for the

387 three model-based SM products are shown in Fig. 9a as well. All three products do not show significant trend

388 in warm seasons as the SM_{AA-min}, while the GLDAS Noah and MERRA2 products show a wetting trend in

389 cold seasons that disagree with the SM_{AA-min}.

390 Fig. 10b shows the time series of SM_{AA-min} and daily SM data derived from the three products for the

391 Shiquanhe network area during the period between August 2010 and August 2018, and the corresponding

392 error statistics are given in Table 5 as well. Although the three products generally capture the seasonal

393 variations of the SM_{AA-min}, both GLDAS Noah and MERRA2 products overestimate the SM_{AA-min} for the

394 entire study period leading to positive bias values, and overestimation is also noted for the ERA5-land product

395 in the warm season with bias of about 0.002 m^3 m^{-3}. The trend analysis for the three SM products are also

396 shown in Fig. 9b. Both the ERA5-land and MERRA2 products are able to reproduce the wetting trend found

397 for the SM_{AA-min}, while the GLDAS Noah product cannot capture well the trend.

398 In summary, the currently model-based SM products still show deficiencies in representing the trend and

399 variation of measured SM dynamics for a long-term period (~10 years) in the Tibetan grassland and desert

400 ecosystems that dominate the landscape of the TP.

401 **5 Discussion**

402 As shown in previous sections, the number of available SM monitoring sites in the Tibet-Obs generally

403 changes with time. For instance, several monitoring sites of the Maqu network located in the wetter area were

404 damaged since 2013, and four new monitoring sites were installed in the drier area in 2015 that would affect

405 the trend of SM time series (i.e. $SM_{AA-valid}$ shown in Section 4.2). On the other hand, the 10-year upscaled

406 SM data (i.e. SM_{AA-min}) produced in this study utilizing three and four monitoring sites with long-term

407 continuous measurements would yield RMSEs of about 0.022 and 0.011 m^3 m^{-3} for the Maqu and Shiquanhe

408 networks, respectively (see Section 4.1). Therefore, to provide a higher-quality continuous SM time series

409 for the future, it is necessary to find an appropriate strategy to maintain the monitoring sites of Tibet-Obs.

410 This section discusses the possible strategies for the Maqu and Shiquanhe networks as examples.

411 At first, a sensitivity analysis is conducted to quantify the impact of the number of monitoring sites on the

412 regional SM estimate. The SM time series described in Section 4.1 (i.e. 11/2009-10/2010 for the Maqu

413 network and 8/2018-7/2019 for the Shiquanhe network) are used to test the sensitivity, and there are totally

414 17 and 12 available monitoring sites for the Maqu and Shiquanhe networks, respectively. Taking the Maqu

415 network as an example, we randomly pick different numbers of sites from 1 to 16 among the 17 sites to make

416 up different combinations, and then compute the RMSEs of the averaged SM obtained by these combinations

417 (Famiglietti et al., 2008; Zhao et al., 2013). These RMSEs are further grouped into nine levels ranging from

418 0.004 to 0.02 m^3 m^{-3}, and the percentage of the combinations falling into each level is summarized in Table

419   6. In general, the percentage increases with increasing number of monitoring sites at any RMSE levels. It can

420   be noted that more than 50% of combinations are able to comply with the RMSE requirement of 0.004 m^3

421   m^{-3} if the number of available monitoring sites are 16 and 11 in the Maqu and Shiquanhe networks,

422   respectively. If the number of available monitoring sites are not less than 13 and 6 in the Maqu and Shiquanhe

423   networks, there would be about 60% of combinations with 13 sites (6 sites) are able to comply with the

424   RMSE requirement of 0.01 m^3 m^{-3}. For the RMSE requirement of 0.02 m^3 m^{-3}, more than 50% of

425   combinations would achieve the requirement if the number of available monitoring sites are not less 7 and 3

426   in the two networks, respectively. In summary, the number of monitoring sites required to maintain current

427   networks depends on the defined RMSE requirement.

428   As shown in Section 4.1, the usage of a minimum number of sites (i.e. three for Maqu and four for Shiquanhe)

429   with about 10-year continuous measurements yields RMSEs of 0.022 and 0.011 m^3 m^{-3} for the Maqu and

430   Shiquanhe networks, respectively. Since there are still 12 monitoring sites providing SM measurements for

431   both networks until 2019 (see Tables 2 and 3), it is possible to decrease the RMSEs if the monitoring sites

432   selected for maintaining are appropriately determined. For the Shiquanhe network, the optimal strategy is to

433   keep the current 12 monitoring sites, which is exactly the combination used in Section 4.1. For the Maqu

434   network, it can be found that there is about 3.52% of combinations with 12 sites could yield the lowest RMSE

435   of 0.006 m^3 m^{-3} (see Table 6). In order to find the optimal combination with 12 sites for the Maqu network,

436   all the possible combinations (i.e. the number of 6188) are ranked by RMSE values from the smallest to

437   largest, and Table 7 lists the examples of ranking 1-5th and 95-100th. It can be noted that the 100th combination

438   contains the largest number of currently available monitoring sites (i.e. 7 sites including CST03, CST05,

439   NST01, NST03, NST05, NST06, and NST10) with a RMSE of less than 0.006 m^3 m^{-3}. Therefore, the 100th

440   combination of 12 monitoring sites (as shown in Table 7) is suggested for the Maqu network.

441   In summary, it is suggested to maintain well current 12 monitoring sites for the Shiquanhe network, while

442   for the Maqu network it is suggested to restore five old monitoring sites, i.e. CST02, NST11, NST13, NST14,

443   and NST15.

444   **6 Data availability**

445   The 10-year (2009-2019) surface SM dataset is freely available from the 4TU.ResearchData repository at

446   https://doi.org/10.4121/uuid:21220b23-ff36-4ca9-a08f-ccd53782e834 (Zhang et al., 2020). The original *in*

447   *situ* SM data, the upscaled SM data, and the supplementary data are stored in .xlsx files. A user guide

448   document is given to introduce the content of the dataset, the status of the Tibet-Obs, and the online dataset

449   utilized in the study.

450   **7 Conclusions**

451   In this paper, we report on the status of the Tibet-Obs and present the long-term *in situ* SM and spatially

452   upscaled SM dataset for the period 2009-2019. In general, the number of available SM monitoring sites

453   decreased over time due to damage of sensors. Until 2019, there are only three and four sites that provide an

454   approximately 10-year consistent SM time series for the Maqu and Shiquanhe networks, respectively.

455   Comparisons between four upscaling methods, i.e. arithmetic averaging (AA), Voronoi diagram (VD), time

456   stability (TS), and apparent thermal inertia (ATI), show that the AA method with input of the maximum

457   number of available SM monitoring sites (AA-max) can be used to represent the actual areal SM conditions

458   (SM_{truth}). The arithmetic average of the three and four monitoring sites with long-term continuous

459   measurements (AA-min) are found to be the most suitable to produce the upscaled SM dataset for the period

460   2009-2019, which may yield RMSEs of 0.022 and 0.011 m^3 m^{-3} for the Maqu and Shiquanhe networks in

461   comparison to the SM_{truth}.

462   Trend analysis of the approximately 10-year upscaled SM time series produced by the AA-min (SM_{AA-min})

463   shows that the Shiquanhe network area in the western part of the TP is getting wet while there is not

464   significant trend found for the Maqu network area in the east. The usage of all the available monitoring sites

465   in each year leads to inconsistent time series of SM that cannot capture well the trend of SM_{AA-min}.

466   Comparisons between the SM_{AA-min} and the model-based SM products from the ERA5-land, GLDAS Noah,

467   and MERRA2 further demonstrate that current model-based SM products still show deficiencies in

468   representing the trend and variation of measured SM dynamics on the TP. Moreover, strategies for

469   maintaining the Tibet-Obs are provided, and it is suggested to maintain well current 12 monitoring sites for

470   the Shiquanhe network, while for the Maqu network it is suggested to restore five old monitoring sites.

471   The 10-year (2009-2019) surface SM dataset presented in this paper includes the 15-min *in situ* measurements

472   taken at a depth of 5 cm collected from three regional-scale networks (i.e. Maqu, Naqu, and Ngari including

473   Ali and Shiquanhe) of the Tibet-Obs, and the spatially upscaled SM datasets produced by the AA-min for

474   the Maqu and Shiquanhe networks. This dataset is valuable for calibrating/validating long-term satellite- and

475   model-based SM products, evaluation of SM upscaling methods, development of data fusion methods, and

476   quantifying the coupling strength between precipitation and SM at 10-year scale.

477   **Author contribution**

478   Pei Zhang, Donghai Zheng, Rogier van der Velde and Zhongbo Su designed the framework of this work. Pei

479   Zhang performed the computations and data analysis, and written the manuscript. Donghai Zheng, Rogier

480   van der Velde and Zhongbo Su supervised the progress of this work and provided critical suggestions, and

481   revised the manuscript. Zhongbo Su and Jun Wen designed the setup of Tibet-Obs, Yijian Zeng, XinWang

482   and Zuoliang Wang involved in maintaining the Tibet-Obs and downloading the original measurements. Pei

483   Zhang, Zuoliang Wang, and Jiali Chen organized the data.

484   **Competing interests**

485   The authors declare that they have no conflict of interest.

486 **Acknowledgments**

487 This study was supported by the Strategic Priority Research Program of Chinese Academy of Sciences (Grant

488 No. XDA20100103) and National Natural Science Foundation of China (Grant No. 41971308, 41871273).

489 **Reference**

490
491 Albergel, C., Dutra, E., Munier, S., Calvet, J. C., Muñoz Sabater, J., Rosnay, P. and Balsamo, G.: ERA-5 and
492   ERA-Interim driven ISBA land surface model simulations: Which one performs better?, Hydrology
493   and Earth System Sciences, 22, doi:10.5194/hess-22-3515-2018, 2018.
494 Bi, H. and Ma, J.: Evaluation of simulated soil moisture in GLDAS using in-situ measurements over the
495   Tibetan Plateau, International Geoscience and Remote Sensing Symposium (IGARSS), 2015-
496   Novem, 4825–4828, doi:10.1109/IGARSS.2015.7326910, 2015.
497 Chen, Y., Yang, K., Qin, J., Zhao, L., Tang, W. and Han, M.: Evaluation of AMSR-E retrievals and GLDAS
498   simulations against observations of a soil moisture network on the central Tibetan Plateau, Journal
499   of Geophysical Research Atmospheres, 118(10), 4466–4475, doi:10.1002/jgrd.50301, 2013.
500 Cheng, M., Zhong, L., Ma, Y., Zou, M., Ge, N., Wang, X. and Hu, Y.: A study on the assessment of multi-
501   source satellite soil moisture products and reanalysis data for the Tibetan Plateau, Remote Sensing,
502   11(10), doi:10.3390/rs11101196, 2019.
503 Colliander, A., Jackson, T. J., Bindlish, R., Chan, S., Das, N., Kim, S. B., Cosh, M. H., Dunbar, R. S., Dang,
504   L., Pashaian, L., Asanuma, J., Aida, K., Berg, A., Rowlandson, T., Bosch, D., Caldwell, T., Caylor,
505   K., Goodrich, D., al Jassar, H., Lopez-Baeza, E., Martínez-Fernández, J., González-Zamora, A.,
506   Livingston, S., McNairn, H., Pacheco, A., Moghaddam, M., Montzka, C., Notarnicola, C., Niedrist,
507   G., Pellarin, T., Prueger, J., Pulliainen, J., Rautiainen, K., Ramos, J., Seyfried, M., Starks, P., Su,
508   Z., Zeng, Y., van der Velde, R., Thibeault, M., Dorigo, W., Vreugdenhil, M., Walker, J. P., Wu, X.,
509   Monerris, A., O'Neill, P. E., Entekhabi, D., Njoku, E. G. and Yueh, S.: Validation of SMAP surface
510   soil moisture products with core validation sites, Remote Sensing of Environment, 191, 215–231,
511   doi:10.1016/j.rse.2017.01.021, 2017a.
512 Colliander, A., Jackson, T. J., Bindlish, R., Chan, S., Das, N., Kim, S. B., Cosh, M. H., Dunbar, R. S., Dang,
513   L., Pashaian, L., Asanuma, J., Aida, K., Berg, A., Rowlandson, T., Bosch, D., Caldwell, T., Caylor,
514   K., Goodrich, D., al Jassar, H., Lopez-Baeza, E., Martínez-Fernández, J., González-Zamora, A.,
515   Livingston, S., McNairn, H., Pacheco, A., Moghaddam, M., Montzka, C., Notarnicola, C., Niedrist,
516   G., Pellarin, T., Prueger, J., Pulliainen, J., Rautiainen, K., Ramos, J., Seyfried, M., Starks, P., Su,
517   Z., Zeng, Y., van der Velde, R., Thibeault, M., Dorigo, W., Vreugdenhil, M., Walker, J. P., Wu, X.,
518   Monerris, A., O'Neill, P. E., Entekhabi, D., Njoku, E. G. and Yueh, S.: Validation of SMAP surface
519   soil moisture products with core validation sites, Remote Sensing of Environment, 191, 215–231,
520   doi:https://doi.org/10.1016/j.rse.2017.01.021, 2017b.
521 Dente, L., Vekerdy, Z., Wen, J. and Su, Z.: Maqu network for validation of satellite-derived soil moisture
522   products, International Journal of Applied Earth Observation and Geoinformation, 17, 55–65,
523   doi:https://doi.org/10.1016/j.jag.2011.11.004, 2012a.
524 Dente, L., Su, Z. and Wen, J.: Validation of SMOS soil moisture products over the Maqu and Twente
525   Regions, Sensors (Switzerland), 12(8), 9965–9986, doi:10.3390/s120809965, 2012b.
526 Van doninck, J., Peters, J., De Baets, B., De Clercq, E. M., Ducheyne, E. and Verhoest, N. E. C.: The potential
527   of multitemporal Aqua and Terra MODIS apparent thermal inertia as a soil moisture indicator,
528   International Journal of Applied Earth Observation and Geoinformation, 13(6), 934–941,
529   doi:https://doi.org/10.1016/j.jag.2011.07.003, 2011.
530 Famiglietti, J. S., Ryu, D., Berg, A. A., Rodell, M. and Jackson, T. J.: Field observations of soil moisture
531   variability across scales, Water Resources Research, 44(1), 1–16, doi:10.1029/2006WR005804,
532   2008.
533 Gao, S., Zhu, Z., Weng, H. and Zhang, J.: Upscaling of sparse in situ soil moisture observations by integrating
534   auxiliary information from remote sensing, International Journal of Remote Sensing, 38(17), 4782–
535   4803, doi:10.1080/01431161.2017.1320444, 2017.
536 Gilbert, Richland O, Statistical Methods for Environmental Pollution Monitoring, United States.

537   https://www.osti.gov/biblio/7037501, 1987.

538 GMAO, Global Modeling and Assimilation Office: MERRA-2 tavg1_2d_lnd_Nx: 2d,1-Hourly,Time-
539   Averaged,Single-Level,Assimilation,Land Surface Diagnostics V5.12.4, Accessed: [Data Access
540   Date], Greenbelt, MD, USA, Goddard Earth Sciences Data and Information Services Center (GES
541   DISC),., 2015.

542 Muñoz-Sabater, J., Dutra, E., Balsamo, G., Schepers, D., Albergel, C., Boussetta, S., Agusti-Panareda, A.,
543   Zsoter, E., and Hersbach, H.: ERA5-Land: an improved version of the ERA5 reanalysis land
544   component, Joint ISWG and LSA-SAF Workshop IPMA, Lisbon, 26–28, 2018.

545 Jacobs, J. M., Mohanty, B. P., Hsu, E.-C. and Miller, D.: SMEX02: Field scale variability, time stability and
546   similarity of soil moisture, Remote Sensing of Environment, 92(4), 436–446,
547   doi:https://doi.org/10.1016/j.rse.2004.02.017, 2004.

548 Ju, F., An, R. and Sun, Y.: Immune evolution particle filter for soil moisture data assimilation, Water
549   (Switzerland), 11(2), doi:10.3390/w11020211, 2019.

550 Kang, J., Jin, R., Li, X. and Zhang, Y.: Block Kriging With Measurement Errors: A Case Study of the Spatial
551   Prediction of Soil Moisture in the Middle Reaches of Heihe River Basin, IEEE Geoscience and
552   Remote Sensing Letters, 14(1), 87–91, doi:10.1109/LGRS.2016.2628767, 2017.

553 Li, C., Lu, H., Yang, K., Han, M., Wright, J. S., Chen, Y., Yu, L., Xu, S., Huang, X. and Gong, W.: The
554   evaluation of SMAP enhanced soil moisture products using high-resolution model simulations and
555   in-situ observations on the Tibetan Plateau, Remote Sensing, 10(4), 1–16, doi:10.3390/rs10040535,
556   2018.

557 Liu, J., Chai, L., Lu, Z., Liu, S., Qu, Y., Geng, D., Song, Y., Guan, Y., Guo, Z., Wang, J. and Zhu, Z.:
558   Evaluation of SMAP, SMOS-IC, FY3B, JAXA, and LPRM Soil moisture products over the
559   Qinghai-Tibet Plateau and Its surrounding areas, Remote Sensing, 11(7), doi:10.3390/rs11070792,
560   2019.

561 Mann, H. B.: Nonparametric Tests Against Trend, Econometrica, 13(3), 245–259, doi:10.2307/1907187,
562   1945.

563 Moghaddam, M., Clewley, D., Silva, A. and Akbar, R.: The SoilSCAPE Network Multiscale In-situ Soil
564   Moisture Measurements: Innovations in Network Design and Approaches to Upscaling in Support
565   of SMAP, in AGU Fall Meeting Abstracts, vol. 2014, pp. IN11A-3599, AA(The Ming Hsieh Dept.
566   of Electr. Eng., University of Southern California, Los Angeles, CA, United States), AB(The Ming
567   Hsieh Dept. of Electr. Eng., University of Southern California, Los Angeles, CA, United States),
568   AC(The Ming Hsieh Dept. of Electr. En. [online] Available from:
569   https://ui.adsabs.harvard.edu/abs/2014AGUFMIN11A3599M, 2014.

570 Qin, J., Yang, K., Lu, N., Chen, Y., Zhao, L. and Han, M.: Spatial upscaling of in-situ soil moisture
571   measurements based on MODIS-derived apparent thermal inertia, Remote Sensing of Environment,
572   138, 1–9, doi:10.1016/j.rse.2013.07.003, 2013.

573 Qin, J., Zhao, L., Chen, Y., Yang, K., Yang, Y., Chen, Z. and Lu, H.: Inter-comparison of spatial upscaling
574   methods for evaluation of satellite-based soil moisture, Journal of Hydrology, 523, 170–178,
575   doi:10.1016/j.jhydrol.2015.01.061, 2015.

576 Rodell, M., Houser, P. R., Jambor, U., Gottschalck, J., Mitchell, K., Meng, C. J., Arsenault, K., Cosgrove,
577   B., Radakovich, J., Bosilovich, M., Entin, J. K., Walker, J. P., Lohmann, D. and Toll, D.: The Global
578   Land Data Assimilation System, Bulletin of the American Meteorological Society, 85(3), 381–394,
579   doi:10.1175/BAMS-85-3-381, 2004.

580 Sen, P. K.: Estimates of the Regression Coefficient Based on Kendall's Tau, Journal of the American
581   Statistical Association, 63(324), 1379–1389, doi:10.1080/01621459.1968.10480934, 1968.

582 Su, Z., Wen, J., Dente, L., Van Der Velde, R., Wang, L., Ma, Y., Yang, K. and Hu, Z.: The tibetan plateau
583   observatory of plateau scale soil moisture and soil temperature (Tibet-Obs) for quantifying
584   uncertainties in coarse resolution satellite and model products, Hydrology and Earth System
585   Sciences, 15(7), 2303–2316, doi:10.5194/hess-15-2303-2011, 2011.

586 Su, Z., De Rosnay, P., Wen, J., Wang, L. and Zeng, Y.: Evaluation of ECMWF's soil moisture analyses using
587   observations on the Tibetan Plateau, Journal of Geophysical Research Atmospheres, 118(11), 5304–
588   5318, doi:10.1002/jgrd.50468, 2013.

589 Tarantola, A.: Inverse Problem Theory and Methods for Model Parameter Estimation, Society for Industrial
590   and Applied Mathematics., 2005.

591 Topp, G. C., Davis, J. L. and Annan, A. P.: Electromagnetic determination of soil water content:
592   Measurements in coaxial transmission lines, Water Resources Research, 16(3), 574–582,

doi:https://doi.org/10.1029/WR016i003p00574, 1980.

Vachaud, G., Passerat De Silans, A., Balabanis, P. and Vauclin, M.: Temporal Stability of Spatially Measured Soil Water Probability Density Function1, Soil Science Society of America Journal, 49, 822–828, doi:10.2136/sssaj1985.03615995004900040006x, 1985.

van der Velde, R.: Soil moisture remote sensing using active microwaves and land surface modelling, 1 January., 2010.

van der Velde, R., Su, Z. and Wen, J.: Roughness determination from multi-angular ASAR Wide Swath mode observations for soil moisture retrieval over the Tibetan Plateau, Proceedings of the European Conference on Synthetic Aperture Radar, EUSAR, Proceeding(August 2011), 163–165, 2014.

Veroustraete, F., Li, Q., Verstraeten, W. W., Chen, X., Bao, A., Dong, Q., Liu, T. and Willems, P.: Soil moisture content retrieval based on apparent thermal inertia for Xinjiang province in China, International Journal of Remote Sensing, 33(12), 3870–3885, doi:10.1080/01431161.2011.636080, 2012.

Wang, J., Ge, Y., Song, Y. and Li, X.: A Geostatistical Approach to Upscale Soil Moisture With Unequal Precision Observations, IEEE Geoscience and Remote Sensing Letters, 11(12), 2125–2129, doi:10.1109/LGRS.2014.2321429, 2014.

Wei, Z., Meng, Y., Zhang, W., Peng, J. and Meng, L.: Downscaling SMAP soil moisture estimation with gradient boosting decision tree regression over the Tibetan Plateau, Remote Sensing of Environment, 225(February), 30–44, doi:10.1016/j.rse.2019.02.022, 2019.

Yang, K., Chen, Y., He, J., Zhao, L., Lu, H. and Qin, J.: Development of a daily soil moisture product for the period of 2002-2011 in Mainland China., Science China Earth Sciences, doi:10.1007/s11430-019-9588-5, 2020.

Zeng, J., Li, Z., Chen, Q., Bi, H., Qiu, J. and Zou, P.: Evaluation of remotely sensed and reanalysis soil moisture products over the Tibetan Plateau using in-situ observations, Remote Sensing of Environment, 163, 91–110, doi:https://doi.org/10.1016/j.rse.2015.03.008, 2015.

Zeng, Y., Su, Z., Van Der Velde, R., Wang, L., Xu, K., Wang, X. and Wen, J.: Blending satellite observed, model simulated, and in situ measured soil moisture over Tibetan Plateau, Remote Sensing, 8(3), 1–22, doi:10.3390/rs8030268, 2016.

Zhang, Q., Fan, K., Singh, V. P., Sun, P. and Shi, P.: Evaluation of Remotely Sensed and Reanalysis Soil Moisture Against In Situ Observations on the Himalayan-Tibetan Plateau, Journal of Geophysical Research: Atmospheres, 123(14), 7132–7148, doi:10.1029/2017JD027763, 2018.

Zhao, H., Zeng, Y., Lv, S. and Su, Z.: Analysis of soil hydraulic and thermal properties for land surface modeling over the Tibetan Plateau, Earth System Science Data, 10(2), 1031–1061, doi:10.5194/essd-10-1031-2018, 2018.

Zhao, L., Yang, K., Qin, J., Chen, Y., Tang, W., Montzka, C., Wu, H., Lin, C., Han, M. and Vereecken, H.: Spatiotemporal analysis of soil moisture observations within a Tibetan mesoscale area and its implication to regional soil moisture measurements, Journal of Hydrology, 482, 92–104, doi:10.1016/j.jhydrol.2012.12.033, 2013.

Zhao, W., Li, A., Jin, H., Zhang, Z., Bian, J. and Yin, G.: Performance evaluation of the triangle-based empirical soil moisture relationship models based on Landsat-5 TM data and in situ measurements, IEEE Transactions on Geoscience and Remote Sensing, 55(5), 2632–2645, doi:10.1109/TGRS.2017.2649522, 2017.

Zheng, D., van der Velde, R., Su, Z., Wang, X., Wen, J., Booij, M. J., Hoekstra, A. Y. and Chen, Y.: Augmentations to the Noah Model Physics for Application to the Yellow River Source Area. Part I: Soil Water Flow, Journal of Hydrometeorology, 16(6), 2659–2676, doi:10.1175/JHM-D-14-0198.1, 2015a.

Zheng, D., van der Velde, R., Su, Z., Wang, X., Wen, J., Booij, M. J., Hoekstra, A. Y. and Chen, Y.: Augmentations to the Noah Model Physics for Application to the Yellow River Source Area. Part II: Turbulent Heat Fluxes and Soil Heat Transport, Journal of Hydrometeorology, 16(6), 2677–2694, doi:10.1175/JHM-D-14-0199.1, 2015b.

Zheng, D., van der Velde, R., Wen, J., Wang, X., Ferrazzoli, P., Schwank, M., Colliander, A., Bindlish, R. and Su, Z.: Assessment of the SMAP Soil Emission Model and Soil Moisture Retrieval Algorithms for a Tibetan Desert Ecosystem, IEEE Transactions on Geoscience and Remote Sensing, 56(7), 3786–3799, doi:10.1109/TGRS.2018.2811318, 2018a.

Zheng, D., Wang, X., van der Velde, R., Ferrazzoli, P., Wen, J., Wang, Z., Schwank, M., Colliander, A., Bindlish, R. and Su, Z.: Impact of surface roughness, vegetation opacity and soil permittivity on L-

649   band microwave emission and soil moisture retrieval in the third pole environment, Remote Sensing
650   of Environment, 209(November 2017), 633–647, doi:10.1016/j.rse.2018.03.011, 2018b.
651 Zheng, D., Wang, X., van der Velde, R., Schwank, M., Ferrazzoli, P., Wen, J., Wang, Z., Colliander, A.,
652   Bindlish, R. and Su, Z.: Assessment of Soil Moisture SMAP Retrievals and ELBARA-III
653   Measurements in a Tibetan Meadow Ecosystem, IEEE Geoscience and Remote Sensing Letters,
654   16(9), 1407–1411, doi:10.1109/lgrs.2019.2897786, 2019.
655

656

657 **Fig. 1. Locations of the Tibet-Obs including Maqu, Naqu, and Ngari (including Ali and Shiquanhe) soil moisture**
658 **monitoring networks. The weather stations of Maqu and Shiquanhe operated by the China Meteorological**
659 **Administration (CMA) are also shown. (Base map is from Esri, Copyright: © Esri)**

(a) Maqu

660
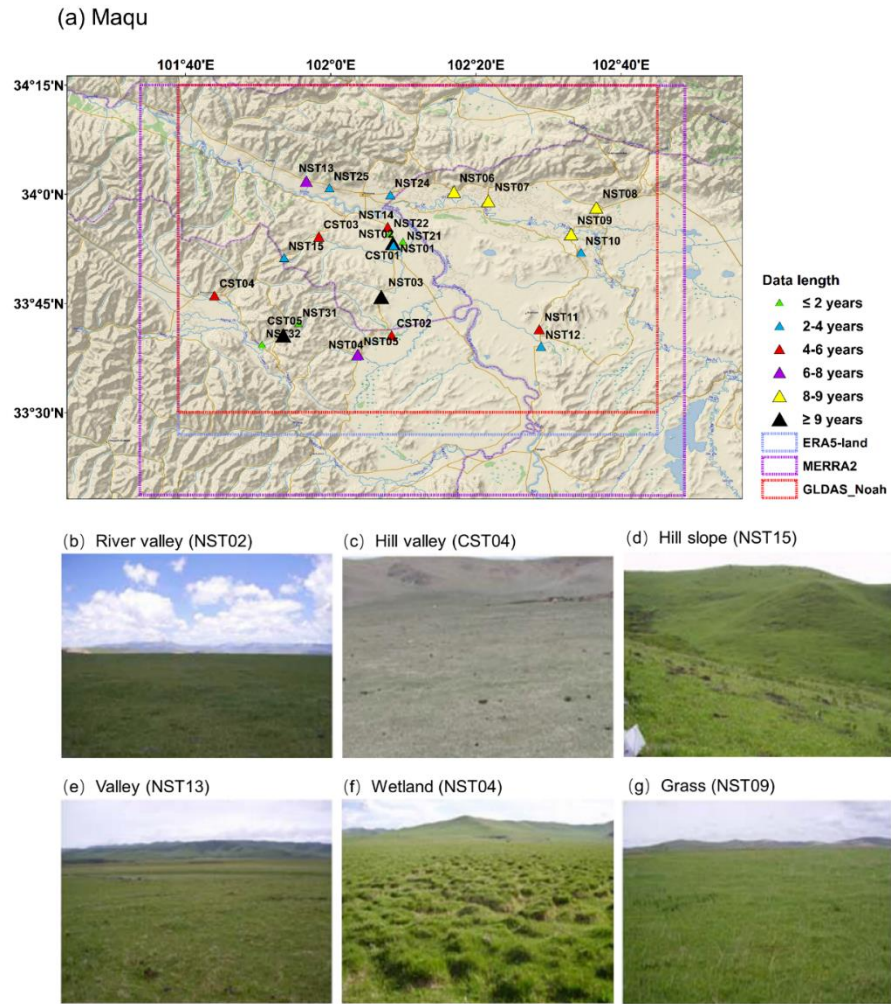
Fig. 2. (a) Overview of the Maqu monitoring network, and typical characteristics of topography and land cover
within the network: (b) river valley, (c) hill valley, (d) hill slope, (e) valley, (f) wetland and (g) grass. The colored
triangles in (a) represent different data lengths of surface SM measurements for each site, and the colored boxes
represent the coverage of selected model-based products. The site name in the bracket in (b)-(g) indicates the site
location for which the photograph is selected. (Base map copyright: ©2018 Garmin)

666
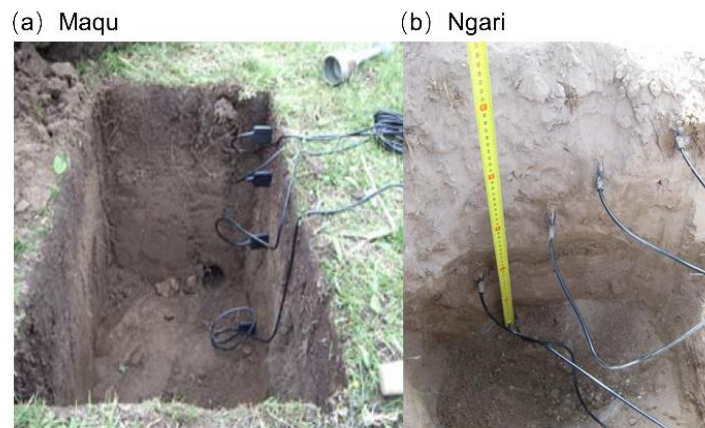
Fig. 3. Examples of typical installation of sensors in monitoring sites of (a) Maqu and (b) Ngari networks.
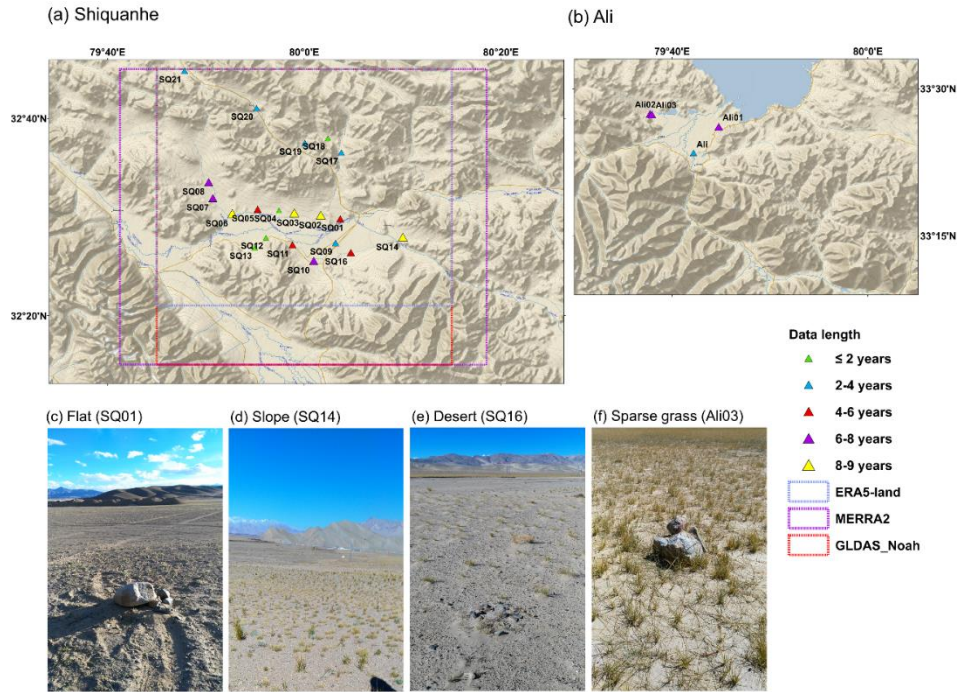
668

669 **Fig. 4. Overview of the Ngari monitoring network including (a) Shiquanhe and (b) Ali networks, and typical**
670 **characteristics of topography and land cover within the network: (c) flat, (d) slope, (e) desert, and (f) sparse grass.**
671 **The colored triangles in (a) and (b) represent different data lengths of surface SM measurements for each site,**
672 **and the colored boxes represent the coverage of selected model-based products. The site name in the bracket in**
673 **(c)-(f) indicates the site location for which the photograph is selected. (Base map copyright: ©2018 Garmin)**
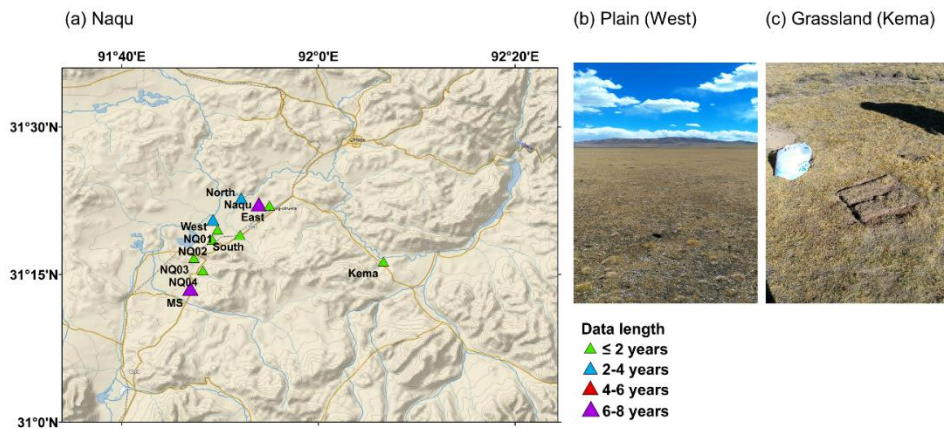
674

675 **Fig. 5. (a) Overview of the Naqu monitoring network, and typical characteristics of topography and land cover**
676 **within the network: (b) plain and (c) grassland. The colored triangles in (a) represent different data lengths of**
677 **surface SM measurements for each site. The site name in the bracket in (b) and (c) indicates the site location for**
678 **which the photograph is selected. (Base map copyright: ©2018 Garmin)**

679
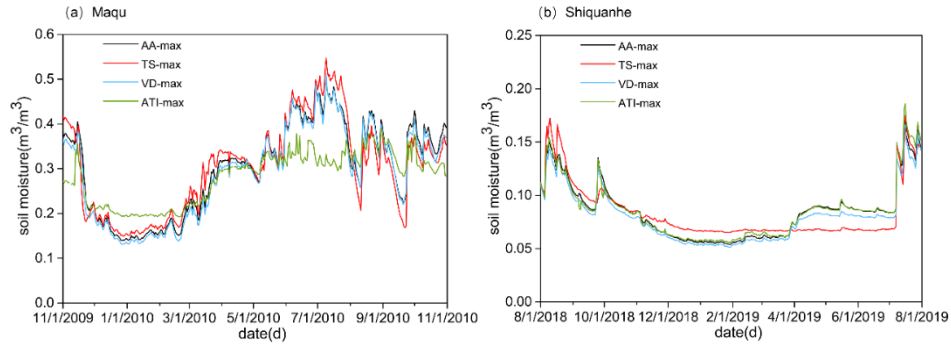
680

681 **Fig. 6. Comparisons of daily average SM for the (a) Maqu and (b) Shiquanhe networks produced by the four**
682 **upscaling methods with input of the maximum number of available SM monitoring sites.**
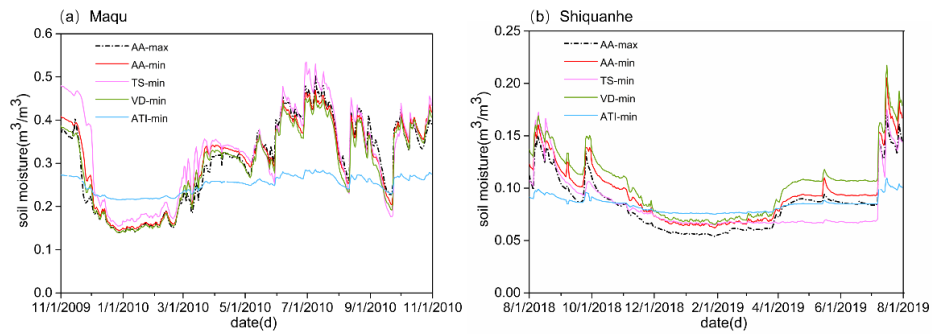
683

684 **Fig. 7. Comparisons of daily average SM for the (a) Maqu and (b) Shiquanhe networks produced by the four**
685 **upscaling methods with input of the minimum number of available SM monitoring sites.**
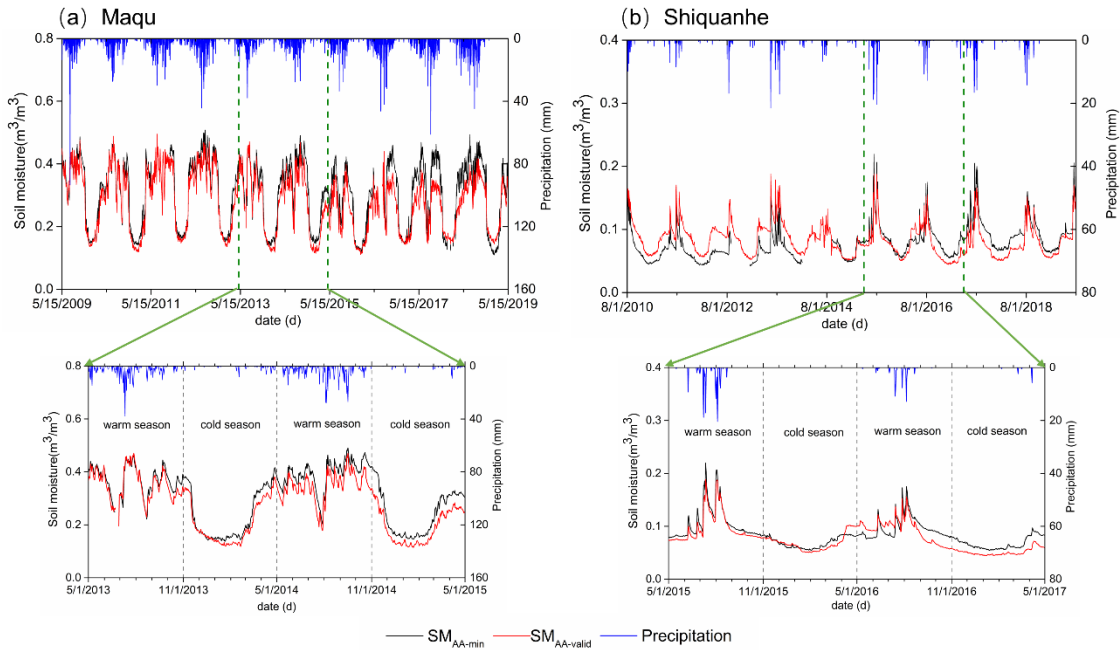
686

687 **Fig. 8. Temporal variation of SM$_{AA-min}$, SM$_{AA-valid}$, and precipitation for the (a) Maqu and (b) Shiquanhe networks**
688 **in a 10-year period as well as the subplot with a 2-year period.**

689
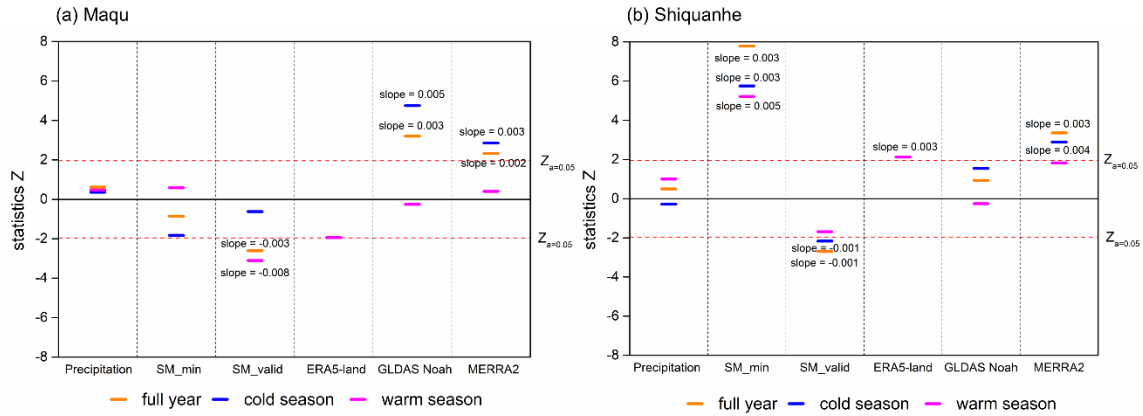
Fig. 9. Mann Kendall trend test and Sen's slope estimate for precipitation, SM$_{AA-min}$, SM$_{AA-valid}$, and model-based
SM derived from the ERA5-land, GLDAS Noah, and MERRA2 for the (a) Maqu and (b) Shiquanhe networks in
a 10-year period.

693
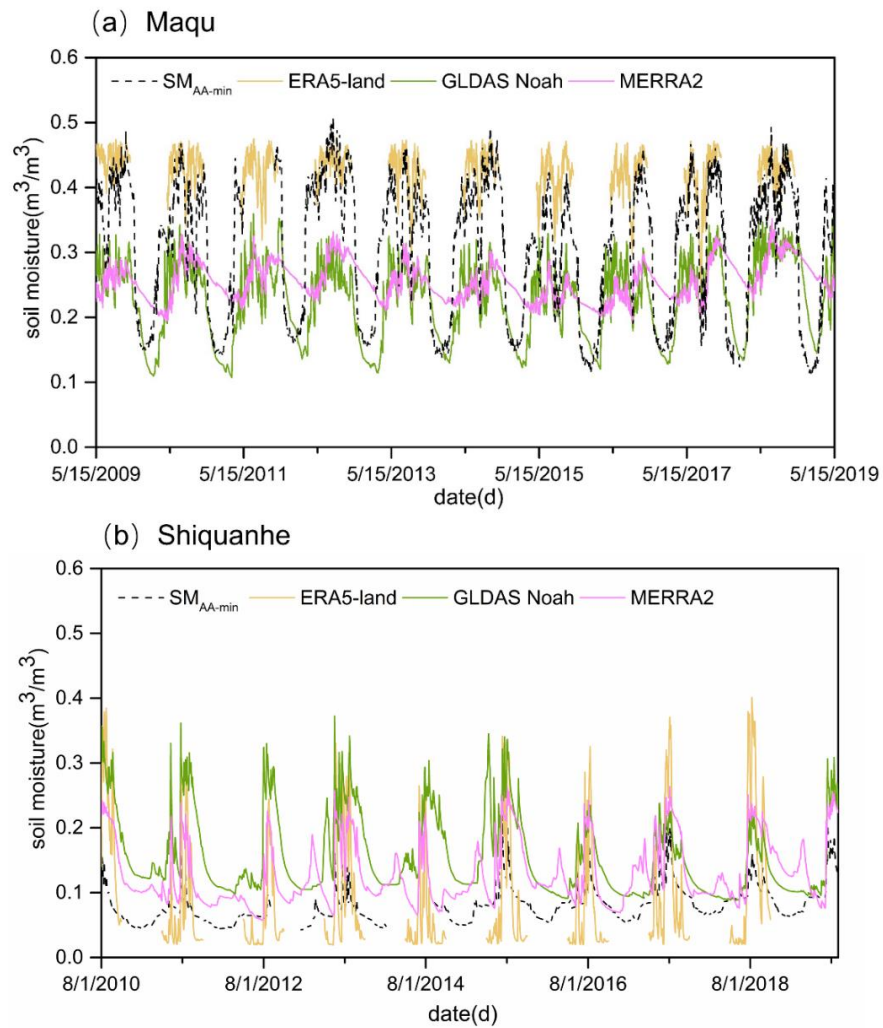
Fig. 10. Comparisons between the model-based SM derived from the ERA5-land, MERRA2, and GLDAS Noah
products and the upscaled SM (SM$_{AA-min}$) for the (a) Maqu and (b) Shiquanhe networks in a 10-year period.

696 **Table 1. Summary of the main Tibet-Obs applications and corresponding findings.**

Literature	*In situ* data	Satellite- and/or model-based products	Key findings
Dente et al. (2012a)	Maqu network, period between 2008 and 2009	LPRM AMSR-E SM product, ASCAT SM product	i) The weighted average of SM depended on the percentage spatial coverage strata can be regarded as the ground reference. ii) The AMSR-E and ASCAT products are able to provide reasonable area SM during monsoon seasons.
Dente et al. (2012b)	Maqu network, period of 2010	Soil Moisture and Ocean Salinity (SMOS) Level 2 SM product	The SMOS product exhibits a systematic dry bias (0.13 m^3 m^{-3}) at the Maqu network.
Zeng et al. (2015)	Maqu network, period between 2008 and 2010	SMOS Level 3 SM product (version 2.45), Advanced Microwave Scanning Radiometer for Earth Observation System SM products (AMSR-E) SM products developed by National Aeronautics and Space Administration (NASA version 6), Land Parameter Retrieval Model (LPRM version 2), and Japan Aerospace Exploration Agency (JAXA version 700), AMSR2 Level 3 SM product (version 1.11), Advanced Scatterometer SM product (ASCAT version TU-Wien-WARP 5.5), ERA-Interim SM product (version 2.0), and Essential Climate Variable SM product (ECV version 02.0)	i) The ECV and ERA products give the best performance, and all products are able to capture the SM dynamic except for the NASA product. ii) The JAXA AMSR-E/AMSR2 products underestimate SM, while the ASCAT product overestimates it. iii) The SMOS product exhibits big noise and bias, and the LPRM AMSR-E product shows a significantly larger seasonal amplitude.
Zheng et al. (2015a)	Maqu network, period between 2009 and 2010	Noah LSM (land surface model) simulations	The modified hydraulic parameterization is able to resolve the SM underestimation in the upper soil layer under wet conditions, and it also leads to better capture for SM profile dynamics combined with the modified root distribution.
Bi & Ma (2015)	Maqu network, period between 2008 and 2011	GLDAS SM products produced by Noah, Mosaic CLM and Variable Infiltration Capacity (VIC) models	The SM simulated by the four LSMs can give reasonable SM dynamics but still show negative biases probably resulted from the high soil organic carbon content.
Li et al. (2018)	Maqu network, period between 2015 and 2016	Soil Moisture Active Passive (SMAP) Level 3 standard (36km) and enhanced (9km) passive SM products (version 3), Community Land Model (CLM4.5) simulations	i) The standard and enhanced SMAP products have similar performance for SM spatial distributions. ii) The SM of enhanced SMAP product exhibits good agreement with the CLM4.5 SM simulation.
Zhao et al. (2017)	Maqu network, period between 2008 and 2010	Downscaled SM from five typical triangle-based empirical SM relationship models	The model treating the surface SM as a second-order polynomial with LST, vegetation indices, and surface albedo outperforms other models.
Ju et al. (2019)	Maqu network, period of 2012	VIC LSM simulations	The IEPFM (immune evolution particle filter with Markov chain Monte Carlo simulation) is able to mitigate particle impoverishment and provide better assimilation results.
Zheng et al. (2018b)	Ngari network, period between 2015 and 2016	SMAP Level 2 radiometer SM product	Modifying surface roughness and employing soil temperature and texture information can improve the SMAP SM retrievals for the desert ecosystem of the TP.
Zhang et al. (2018)	Maqu and Ngari networks, period between 2010 and 2013	ERA-Interim SM product, MERRA SM product, GLDAS_Noah SM product (version2.0 and version2.1)	All these products exhibit overestimation at the Ngari network while underestimation at the Maqu network except for the ERA-Interim product.

Zheng et al. (2018a)	Maqu and Ngari networks, period between 2015 and 2016	SMAP Level 1C radiometer brightness temperature products (version 3)	i) The SMAP algorithm underestimates the significance of surface roughness while overestimates the impact of vegetation. ii) The modified brightness temperature simulation can result in better SM retrievals.
Wei et al. (2019)	Maqu and Ngari networks, period between 2015 and 2016	SMAP Level 3 SM passive product	The downscaled SM still can keep accuracy compared to the SM of original SMAP product.
Liu et al. (2019)	Maqu and Ngari networks, period between 2012 and 2016	SMAP Level 3 SM products (version 4.00), SMOS-IC SM products (version 105), Fengyun-3B Microwave Radiation Image SM product (FY3B MWRI), JAXA AMSR2 Level 3 SM product, LPRM AMSR2 Level 3 SM product (version 3.00)	i) The JAXA AMSR2 product underestimates area SM while the LPRM AMSR2 product overestimates it. ii) The SMOS-IC product exhibits some noise of SM temporal variation. iii) The SMAP product has the highest accuracy among the five products while FY3B shows relatively lower accuracy.
Yang et al. (2020)	Maqu and Ngari network, period between 2008 and 2011	AMSR-E brightness temperature product	The assimilated SM products exhibit higher accuracy than the AMSR-E product and LSM simulations for wet areas, whereas their accuracy is similar for dry areas.
Su et al. (2013)	Maqu and Naqu networks, period between 2008 and 2009.	AMSR-E SM product, ASCAT Level 2 SM product, ECMWF SM analyses i.e. optimum interpolation and extended Kalman filter products	i) The Naqu area SM is overestimated by the ECMWF products in monsoon seasons, while the Maqu area SM produced by the ECMWF is comparable to previous studies. ii) The SM estimate cannot be considerably improved by assimilating ASCAT data due to the CDF matching approach and the data quality.
Zeng et al. (2016)	Maqu, Naqu and Ngari networks, period between 2010 and 2011	LPRM AMSR-E SM product, ERA-Interim SM product	The blended SM is able to capture temporal variations across different climatic zones over the TP.
Cheng et al. (2019)	Maqu, Naqu and Ngari networks, period of 2010	European Space Agency Climate Change Initiative Soil Moisture SM product (ESA CCISM version 4.4), ERA5 SM product	i) The seasonal variation and spatial distribution of SM can be captured by all four products i.e., ESA CCI_active, ESA CCI_passive, ESA CCI_combined, and ERA5. ii) The ESA CCI_active and ESA CCI_combined products exhibit narrower magnitude than the ESA CCI passive and ERA5 products. iii) The SM uptrend across the TP can be found from the ERA5 product.

697

Table 2. Data records of all the SMST monitoring sites performed for the Maqu network. Blank cells represent that there is not measurement performed. Cells with hyphen represent that there is not data missing. The number in cells represents the month(s) when the data is missing for each year.

	2009	2010	2011	2012	2013	2014	2015	2016	2017	2018	2019	Data length (months)
CST01	—	—	10~12	1~6 10~12								36
CST02	—	—	5~12	1~10	6	7~12						46
CST03	—	—	—	—	6~12	1~10	7~12			1~9	5~12	68
CST04	1~5	—	12	1~3 11~12	1~2 6	8~10	7~12		1~6	7~12		73
CST05	—	—	—	—	6	—	—	5~7	—	1~2	6~12	119
NST01	1~5	—	—	—	6	—	—	5~7	—	—	6~12	116
NST02	1~3	—	—	7~8 10~12								40
NST03	—	—	5~10	—	6	—	—	5~7	—	—	6~12	115
NST04	—	—	10~12									33
NST05	3~5	—	—	—	6~12	1~7	—	5~7	7~12	1~7	6~12	92
NST06	—	1~3 12	1~3	—	6	—	—	6~7	8~12	1~7	6~12	104
NST07	—	—	3	—	6, 12	1	12	1~2 7,12	1~2 12	1~3 9~12		101
NST08	—	2, 4 9~12	1~5	—	6~10	1~10	—	6~7	—	—	6~12	95
NST09	1, 12	1~4 12	1~3	—	1~2 6	7~10	12	1~3 7, 12	1~2 7	—	6~12	99
NST10	—	11~12	1~5 7~12	1~6	6~12					1~7	6~12	44
NST11	—	—	—	7~8	6	7~12						63
NST12	10~12	1~9	—	—	6~12	1~10	7~12					49
NST13	—	—	—	—	6	—	7~12					77
NST14	6~9	—	—	—	6	10~12						64
NST15	—	10~12	1~5	6~12								33
NST21						1~7	7~12					11
NST22						1~7	7~12					11
NST24						1~7	2~12	1~7	—	—	6~12	40
NST25						1~7	—	2~12	1~8	—	6~12	39
NST31									1~8	7~12		10
NST32										1~5	6~12	12

Table 3. Same as the Table 2 but for the Ngari network.

	2010	2011	2012	2013	2014	2015	2016	2017	2018	2019	Data length (months)
					Shiquanhe network						
SQ01	1~7	—	—	—	9~12	1~9					52
SQ02	1~7	—	—	—	5~9	—	—	—	—	9~12	104
SQ03	1~7	—	—	—	8~9	—	—	—	—	9~12	107
SQ04	1~7	—	9~12								25
SQ05	1~7	—	—	—	5~12						45
SQ06	1~7	—	9~12	1	2~9	—	—	—	—	9~12	96
SQ07	1~7	—	—	9~12	1~8	—	7~8	7~8	—	9~12	93
SQ08	1~7	8~12		1~8	8~9	—	—	—	—	9~12	82
SQ09	1~7	—	9~12	1~8	9~12						37
SQ10		1~8	—	—	7~12	1~9	7~12	1~8	—	9~12	67
SQ11	1~7	—	—	9~12					1~8	9~12	49
SQ12	1~7	—	9~12								25
SQ13	1~7	8~12									12
SQ14	1~7	—	—	—	6 8~9	—	—	—	—	9~12	106
SQ16	1~7	7~8	—	—	3~8	9~12					53
SQ17							1~8	—	—	9~12	36
SQ18							1~8	1	9~12		23
SQ19							1~8	—	—	9~12	36
SQ20							1~8	—	—	9~12	36
SQ21							1~8	—	—	9~12	36
					Ali network						
Ail	1~7	—	9~12	1~8				1~8	8~12		40
Ali01	1~7	8~12	1~8	—	8	—	—	—	8~12		82
Ali02	1~7 11~12	1~8	—	—	8	—	—	—	8~12		85
Ali03	1~7	—	—	3~12	1~8	—	—	—	8~12		78

Table 4. Same as the Table 2 but for the Naqu network.

	2010	2011	2012	2013	2014	2015	2016	2017	2018	2019	Data length (months)
Naqu	1~7	—	—	8~9	6~8	6~9	—	9~12	1~8	9~12	88
East		1~8	—	9~12							24

West	1~7	1~8	—	1~9	7~12	1~7	8~12				42
North	1~8 11~12	1~3 9	9~12				1~8	9~12	1~8	9~12	42
South		1~8	9~12								12
Kema				1~9	3~9	—	8~12				26
MS	1~7	—	10~12	1~9	8~9 11~12	1~5	—	9~12	1~8	9~12	76
NQ01									1~8	9~12	12
NQ02									1~8	9~12	12
NQ03							1~8	9~12	1~8	9~12	24
NQ04									1~8	9~12	12

705

Table 5. Error statistics computed between the $SM_{AA\text{-}min}$ and the three model-based SM products for the Maqu and Shiquanhe networks.

	Bias ($m^3\,m^{-3}$)	RMSE ($m^3\,m^{-3}$)	Bias ($m^3\,m^{-3}$)	RMSE ($m^3\,m^{-3}$)
	Warm season		Cold season	
	Maqu			
ERA5-land	0.050	0.067	-	-
GLDAS Noah	-0.112	0.125	-0.049	0.088
MERRA2	-0.113	0.124	0.006	0.097
	Shiquanhe			
ERA5-land	0.002	0.079	-	-
GLDAS Noah	0.010	0.116	0.052	0.058
MERRA2	0.054	0.069	0.049	0.053

Table 6. Percentages of each combination's RMSE fall into different levels of defined RMSE requirement.

RMSE	0.004	0.006	0.008	0.010	0.012	0.014	0.016	0.018	0.020
	Maqu network								
n=1 (%)									
n=2 (%)								0.74	3.68
n=3 (%)						0.44	1.32	3.97	7.79
n=4 (%)					0.21	1.05	3.74	9.16	16.93
n=5 (%)				0.03	0.58	3.10	9.31	18.23	28.18
n=6 (%)				0.09	1.87	8.27	19.18	31.22	42.36
n=7 (%)				0.69	6.21	18.11	31.91	43.98	54.32
n=8 (%)			0.08	3.29	14.97	30.32	43.97	55.36	64.79
n=9 (%)			0.84	9.58	26.27	42.42	55.47	65.94	74.16
n=10 (%)		0.01	3.91	19.74	38.94	54.41	66.13	75.21	82.23
n=11 (%)		0.53	11.10	32.92	51.7	65.66	75.9	83.32	88.87

n=12 (%)		3.52	23.95	47.3	64.03	75.87	84.45	90.14	94.30
n=13 (%)	0.29	13.82	39.87	61.81	75.67	85.38	91.55	95.38	97.77
n=14 (%)	3.68	32.35	57.79	74.85	86.47	92.79	96.91	98.82	99.41
n=15 (%)	21.32	56.62	75.00	88.97	95.59	98.53	99.26	100.00	100.00
n=16 (%)	52.94	82.35	94.12	94.12	100.00	100.00	100.00	100.00	100.00
Shiquanhe network									
n=1 (%)							8.33	16.67	25.00
n=2 (%)		1.52	1.52	4.55	13.64	30.30	37.88	42.42	48.48
n=3 (%)		6.82	21.36	25.45	33.18	42.73	53.18	59.55	65.00
n=4 (%)	1.62	11.31	29.7	41.41	51.11	57.37	63.23	70.51	77.58
n=5 (%)	3.66	23.11	36.87	49.12	60.23	68.18	76.14	82.32	88.26
n=6 (%)	11.36	30.95	44.37	59.85	70.24	79.11	85.28	90.15	93.29
n=7 (%)	20.20	39.77	56.06	68.31	77.90	86.87	93.43	96.84	98.48
n=8 (%)	29.29	50.51	62.63	77.58	89.09	96.57	97.98	98.99	99.60
n=9 (%)	33.64	59.55	82.73	91.36	96.36	98.18	99.55	99.55	100.00
n=10 (%)	48.48	78.79	92.42	96.97	96.97	100.00	100.00	100.00	100.00
n=11 (%)	83.33	91.67	100.00	100.00	100.00	100.00	100.00	100.00	100.00

710

Table 7. The combinations of monitoring sites ranked by RMSE values of average SM at the Maqu network.

Rank	Site1	Site2	Site3	Site4	Site5	Site6	Site7	Site8	Site9	Site10	Site11	Site12	**RMSE**
1	CST01	CST02	NST02	NST03	NST04	NST05	NST06	NST07	NST10	NST13	NST14	NST15	0.00402
2	CST01	CST02	CST04	NST01	NST02	NST03	NST04	NST05	NST06	NST07	NST13	NST15	0.00417
3	CST02	NST01	NST02	NST03	NST04	NST05	NST06	NST07	NST10	NST13	NST14	NST15	0.00450
4	CST01	CST02	NST01	NST02	NST03	NST04	NST05	NST06	NST07	NST13	NST14	NST15	0.00450
5	CST01	CST02	CST03	NST02	NST03	NST04	NST05	NST06	NST07	NST10	NST14	NST15	0.00451
96	CST01	CST02	CST03	CST04	CST05	NST03	NST06	NST10	NST11	NST13	NST14	NST15	0.00555
97	CST01	CST02	CST03	NST01	NST02	NST04	NST05	NST06	NST11	NST13	NST14	NST15	0.00555
98	CST01	CST02	CST03	CST04	CST05	NST01	NST02	NST05	NST06	NST10	NST11	NST15	0.00556
99	CST03	NST02	NST03	NST04	NST05	NST06	NST07	NST10	NST11	NST13	NST14	NST15	0.00557
100	**CST02**	**CST03**	**CST05**	**NST01**	**NST03**	**NST05**	**NST06**	**NST10**	**NST11**	**NST13**	**NST14**	**NST15**	**0.00557**

Appendix A. Basic information of the Tibet-Obs

Table A1. Site information of the Maqu network (site name, elevation, topography (TPG), land cover (LC), soil texture at 5-15 cm depth (STX), soil bulk density at 5cm depth (BD), soil organic matter content at 5-15cm depth (OMC), Not Available (NA), BD and OMC values are measured in the laboratory).

Site name	Elevation (m)	TPG	LC	STX	BD (kg m^{-3})	OMC (g/kg)
CST01	3431	River valley	Grass	NA	NA	NA
CST02	3449	River valley	Grass	NA	NA	NA
CST03	3507	Hill valley	Grass	NA	NA	NA
CST04	3504	Hill valley	Grass	NA	NA	NA
CST05	3542	Hill valley	Grass	NA	NA	NA
NST01	3431	River valley	Grass	Silt loam	0.96	18
NST02	3434	River valley	Grass	Silt loam	0.81	18
NST03	3513	Hill slope	Grass	Silt loam	0.63	49
NST04	3448	River valley	Wetland	Silt loam	0.26	229
NST05	3476	Hill slope	Grass	Silt loam	0.75	22
NST06	3428	River valley	Grass	Silt loam	0.81	23
NST07	3430	River valley	Grass	Silt loam	0.58	23
NST08	3473	Valley	Grass	Silt loam	1.06	34
NST09	3434	River valley	Grass	Sandy loam	0.91	17
NST10	3512	Hill slope	Grass	Loam-silt loam	1.05	24
NST11	3442	River valley	Wetland	Organic soil	0.24	136
NST12	3441	River valley	Grass	Silt loam	1.02	39
NST13	3519	Valley	Grass	Silt loam	0.67	29
NST14	3432	River valley	Grass	Silt loam	0.68	30
NST15	3752	Hill slope	Grass	Silt loam	0.78	56
NST21	3428	River valley	Grass	Silt loam	NA	NA
NST22	3440	River valley	Grass	Silt loam	NA	NA
NST24	3446	River valley	Grass	Silt loam	NA	NA
NST25	3600	Hill slope	Grass	Silt loam	NA	NA
NST31	3490	NA	NA	NA	NA	NA
NST32	3490	Hill valley	Grass	NA	NA	NA

Table A2. Soil moisture with temporal persistence for the Maqu network. Light gray shaded cells represent that there is not data missing, dark gray shaded cells represent there is data missing with little influence.

Time	2009.11~2010.11	2010.11~2011.11	2011.11~2012.11	2012.11~2013.11	2013.11~2014.11	2014.11~2015.11	2015.11~2016.11	2016.11~2017.11	2017.11~2018.11
CST05									-
NST01									
NST03									
NST06									
NST07									
NST13									
NST01									
NST14									
CST03									
NST05									
CST01									
CST04									
NST02									
NST04									
CST02									
NST10									
NST15									

Table A3. Same as the Table A1 but for the Ngari network (BD and OMC data are not available).

Site name	Elevation (m)	TPG	LC	STX
			Shiquanhe network	
SQ01	4306	Flat	Desert	Loamy sand
SQ02	4304	Gentle slope	Desert	Sand
SQ03	4278	Gentle slope	Desert (with sparse bushes)	Sand
SQ04	4269	Edge of a wetland	Sparse grass	Loamy sand
SQ05	4261	Edge of a marsh	Sparse grass	Sand
SQ06	4257	Flat	Sparse grass	Loamy Sand
SQ07	4280	Flat	Desert (with sparse bushes)	Sand
SQ08	4306	Flat	Desert	Sand
SQ09	4275	Flat	Desert/river bed	Sand
SQ10	4275	Flat	Grassland	Fine sand with some thick roots
SQ11	4274	Flat	Grassland with bushes	Loamy sand
SQ12	4264	Flat	Edge of riverbed	Sandy loam
SQ13	4292	Flat	Valley bottom	Sand

SQ14	4368	Slope	Desert	Sandy loam
SQ16	4288	Flat	Desert/river bed	Loam
SQ17	4563	NA	NA	NA
SQ18	4634	NA	NA	NA
SQ19	4647	NA	NA	NA
SQ20	4695	NA	NA	NA
SQ21	4606	NA	NA	NA
Ali network				
Ali	4288	Flat	Grass	Loamy sand
Ali01	4262	Flat	Sparse grass	Sand
Ali02	4266	Flat	Sparse grass	Sand
Ali03	4261	Edge of a wetland	Grass	Sand

Table A4. Same as Table A2 but for the Shiquanhe network.

Time	2010.8~ 2011.8	2011.8~ 2012.8	2012.8~ 2013.8	2013.8~ 2014.8	2014.8~ 2015.8	2015.8~ 2016.8	2016.8~ 2017.8	2017.8~ 2018.8	2018.8~ 2019.8
SQ02									
SQ03									
SQ06									
SQ14									
SQ08									
SQ07									
SQ17									
SQ19									
SQ20									
SQ21									
SQ10									
SQ11									

725

Table A5. Same as the Table A1 but for the Naqu network (BD and OMC data are not available).

Site name	Elevation (m)	TPG	LC	STX
Naqu	4509	Plain	Grassland	Loamy sand
East	4527	Flat hill top	Grassland	Loamy sand
West	4506	Plain	Grassland	Loamy sand
North	4507	Slope on riverbank	Grassland	Loamy sand
South	4510	Slope of wetland	Wetland	Loamy sand

Kema	4465	River valley	Grass	Silt loam
MS	4583	NA	NA	NA
NQ01	4517	NA	NA	NA
NQ02	4552	NA	NA	NA
NQ03	4638	NA	NA	NA
NQ04	4632	NA	NA	NA

Appendix B. Spatial upscaling methods

B.1 Arithmetic averaging

The arithmetic averaging method assigns an equal weight coefficient to each SM monitoring site of the
730 network, which can be formulated as:

$$\overline{\theta}_t^{ups} = \frac{1}{N}\sum_{i=1}^{N}\theta_{t,i}^{obs} \tag{B1}$$

where i represents the ith SM monitoring site.

B.2 Voronoi diagram

The Voronoi diagram method divides the network area into several parts according to the distances between
735 each SM monitoring site. This approach determines the weight of each site (w_i [-]) based on the geographic
distribution of all the SM monitoring sites within the network area, which can be formulated as:

$$\overline{\theta}_t^{ups} = \frac{\sum_{i=1}^{N}w_i\theta_{t,i}^{obs}}{\sum_{i=1}^{N}w_i} \tag{B2}$$

B.3 Time stability

The time stability method is based on the assumption that the spatial SM pattern over time tends to be
740 consistent (Vachaud et al., 1985), and the most stable site can be regarded as the representative site of the
network. For each SM monitoring site i within the time window (M days in total), the mean relative
difference MRD_i [-] and standard deviation of the relative difference $\sigma(RD_i)$ [-] are estimated as:

$$\sigma(RD_i) = \sqrt{\frac{1}{M-1}\sum_{t=1}^{M}(RD_{t,i} - MRD_i)^2} \tag{B3}$$

$$MRD_i = \frac{1}{M}\sum_{t=1}^{M}\frac{\theta_{t,i}^{obs}-\overline{\theta_t^{obs}}}{\overline{\theta_t^{obs}}} \tag{B4}$$

745 $$RD_{t,i} = \frac{\theta_{t,i}^{obs}-\overline{\theta_t^{obs}}}{\overline{\theta_t^{obs}}} \tag{B5}$$

where $\theta_{t,i}^{obs}$ [m^3 m^{-3}] represents the SM measured on the tth day at the ith monitoring site, $\overline{\theta_t^{obs}}$ [m^3 m^{-3}]
represents the mean SM measured at all available monitoring sites on the tth day. MRD_i quantifies the bias of
each SM monitoring site to identify a particular location is wetter or drier than regional mean, and $\sigma(RD_i)$

characterizes the precision of the SM measurement. Jacobs et al., (2004) combined above two statistical metrics as a comprehensive evaluation criterion (CEC_i [-]):

$$CEC_i = \sqrt{(MRD_i)^2 + \sigma(RD_i)^2} \tag{B6}$$

The most stable site is identified by the lowest CEC_i value.

B.4 Apparent thermal inertia

The apparent thermal inertia (ATI) method is based on the close relationship between apparent thermal inertia (τ [K^{-1}]) and SM (θ [m^3 m^{-3}]) (Van doninck et al., 2011; Veroustraete et al., 2012). If the true areal SM ($\bar{\theta}_t^{tru}$ [m^3 m^{-3}]) is available, then the weight vector β can be derived by the ordinary least-squares (OLS) method that minimizes the cost function J as:

$$J = \sum_{t=1}^{M}(\theta_t^{tru} - \beta^T \theta_t^{obs})^2 \tag{B7}$$

However, the θ_t^{tru} [m^3 m^{-3}] is usually not available in practice, and the representative SM ($\bar{\theta}_t^{rep}$ [m^3 m^{-3}]) is thus introduced that contains random noise but with no bias. Since the OLS method may results in overfitting with usage of the $\bar{\theta}_t^{rep}$, a regularization term is introduced and Eq. (B7) can be re-formulated as (Tarantola, 2005):

$$J = \sum_{t=1}^{M}(\bar{\theta}_t^{rep} - \beta^T \theta_t^{obs})\sigma^{-2}(\bar{\theta}_t^{rep} - \beta^T \theta_t^{obs}) + R\beta^T \beta \tag{B8}$$

where σ [m^3 m^{-3}] represents the standard deviation of $\bar{\theta}_t^{rep}$, R [-] is the regularization parameter.

The core issue of the ATI approach is to obtain the $\bar{\theta}_t^{rep}$ and minimize the cost function of Eq. (B8) to obtain β and R. The $\bar{\theta}_t^{rep}$ can be retrieved from the apparent thermal inertia τ by the empirical regression g(τ), and τ has strong connection with the surface status, e.g. land surface temperature and albedo, which is defined as:

$$\tau = C\frac{1-a}{A} \tag{B9}$$

where C [-] represents the solar correction factor, a [-] represents the surface albedo, and A [K] represents the amplitude of the diurnal temperature cycle. The albedo and land surface temperature data obtained from the MODIS MCD43A3 and MYD11A1/MOD11A1 Version 6 products are used to derive the ATI according to Eq. (B9) in this study.

The solar correlation factor C in Eq. (B9) is computed as:

$$C = \sin\varphi\sin\delta(1 - tan^2\varphi tan^2\delta)^{1/2} + cos\varphi cos\delta arccos(-tan\varphi tan\delta) \tag{B10}$$

with

$$\delta = 0.00691 - 0.399912\cos(\gamma) + 0.070257\sin(\gamma) - 0.006758\cos(2\gamma) + 0.000907\sin(2\gamma) -$$
$$0.002697\cos(3\gamma) + 0.00148\sin(3\gamma) \tag{B11}$$

and

$$\gamma = \frac{2\pi(n_d - 1)}{365.25} \tag{B12}$$

where φ represents the latitude [rad], δ represents the solar declination [rad], and n_d represents the Julian day number.

The amplitude of the diurnal LST A is estimated as LST_{max} - LST_{min} for a single day. Finally, we use the regression analysis between *in situ* SM measurements (θ) at each monitoring site and corresponding ATI (τ)

785 to obtain the g($\cdot$) form.

There are 17 and 12 monitoring sites participate in the regression analysis for the Maqu and Shiquanhe networks during the periods of 11/2009-10/2010 and 8/2018-7/2019, respectively. The ATI cannot be obtained for each monitoring site in every day since the satellite-based LST data are contaminated by clouds. In order to make full use of the data, we make the ATI-SM pair for the 1st monitoring site on the 1st day as

790 No. 1, the pair for the 17th (or 12th) monitoring site in the Maqu (or Shiquanhe) network on the 1st day as the No. 17 (or No. 12), the pair for the 1st monitoring site at the 2nd day as the No. 18 (No. 13), and so on. Later on, we select a certain number of ATI-SM pairs (e.g. 40, 50, 60, 70, 80, 90, and 100) as a group to compute the averaged ATI and SM and construct the most reasonable regression relationship between them. If the ATI or SM data at one day is missing, this pair is ignored. As shown in Fig. B1, the empirical relationship is

795 generated from 80-pair-averaged ATI and SM for the Maqu and Shiquanhe networks.

When the empirical relationship g($\cdot$) is determined, the regional-average SM can be derived from grid-averaged ATI by the function g($\cdot$), which it is regarded as $\bar{\theta}_t^{rep}$ in Eq. (B8). Finally, the optimal β ($\hat{\beta}$) is obtained by minimizing the cost function (i.e. Eq. (B8)), and the upscaled SM can be estimated as:

$$\bar{\theta}_t^{ups} = \hat{\beta}\theta_t^{obs} \tag{B13}$$

800 The detailed description of the ATI method is referred to Qin et al. (2013).
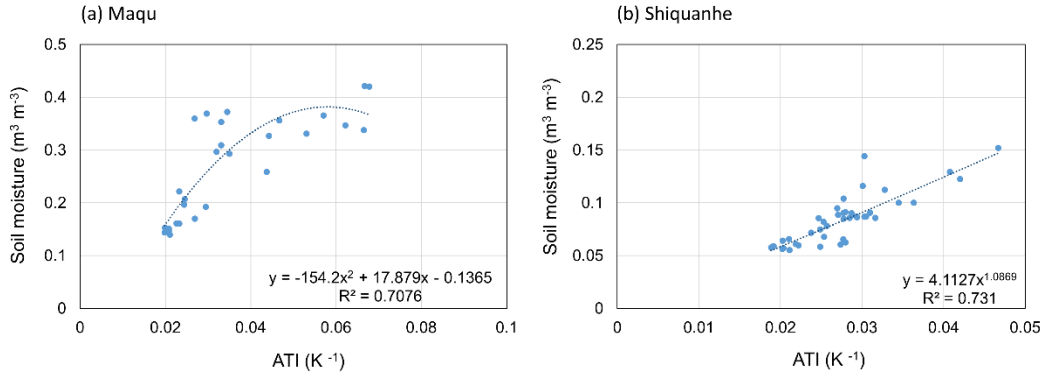
Fig. B1 Empirical relationship between 80-pair-averaged ATI and SM at the (a) Maqu and (b) Shiquanhe networks.
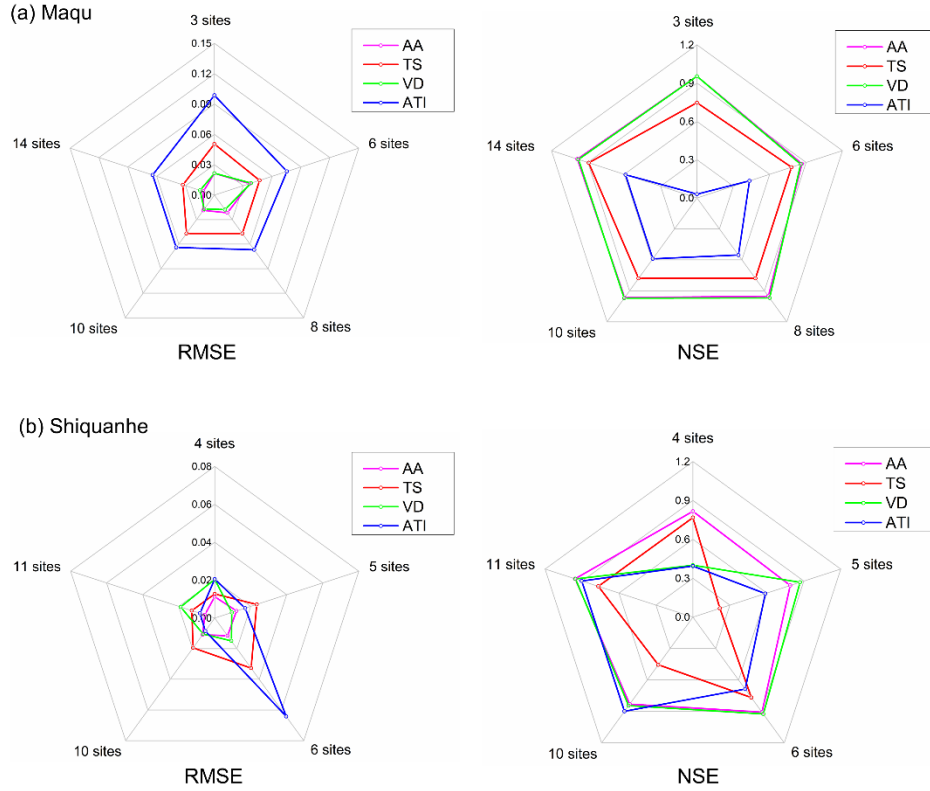
Fig. B2. Radar graph of error statistics (i.e. RMSE and NSE) computed between the SM$_{truth}$ produced by the AA-max and the upscaled SM produced by the four upscaling methods with input of different number of available monitoring sites for the (a) Maqu and (b) Shiquanhe networks.

Table B1. Evaluated metrics computed for the upscaled SM produced by the four upscaling methods with input
810 **of the maximum available monitoring sites.**

Methods	Maqu			Shiquanhe		
	MRD	σ(RD)	CEC	MRD	σ(RD)	CEC
AA-max	0.009	0.054	**0.055**	0.012	0.046	**0.047**
TS-max	0.022	0.089	0.092	0.011	0.114	0.114
VD-max	-0.026	0.064	0.069	-0.042	0.033	0.053
ATI-max	-0.005	0.145	0.145	0.016	0.068	0.070

Table B2. Error statistics computed between the SM obtained by the four upscaling methods with input of the minimum available monitoring sites and the SM$_{truth}$ produced by the AA-max for the Maqu and Shiquanhe networks.

	Bias (m^3 m^{-3})	RMSE(m^3 m^{-3})	ubRMSE(m^3 m^{-3})	NSE
		Maqu		
AA-min	0.005	0.022	0.021	0.954
TS-min	0.025	0.050	0.044	0.747
VD-min	-0.007	0.022	0.020	0.954
ATI-min	-0.052	0.099	0.084	0.030
		Shiquanhe		

AA-min	0.010	0.011	0.005	0.816
TS-min	-0.001	0.013	0.013	0.768
VD-min	0.019	0.020	0.006	0.400
ATI-min	-0.001	0.021	0.021	0.393

815